FUS RRM regulates poly(ADP-ribose) levels after transcriptional arrest and PARP-1 activation on DNA damage

Evgeniya Mamontova, Marie-Jeanne Clément, Maria Sukhanova, Vandana Joshi, Ahmed Bouhss, Juan-Carlos Rengifo-Gonzalez, Bénédicte Desforges, Loic Hamon, Olga Lavrik, David Pastré

Cell Reports

Article

FUS RRM regulates poly(ADP-ribose) levels after transcriptional arrest and PARP-1 activation on DNA damage

Graphical abstract

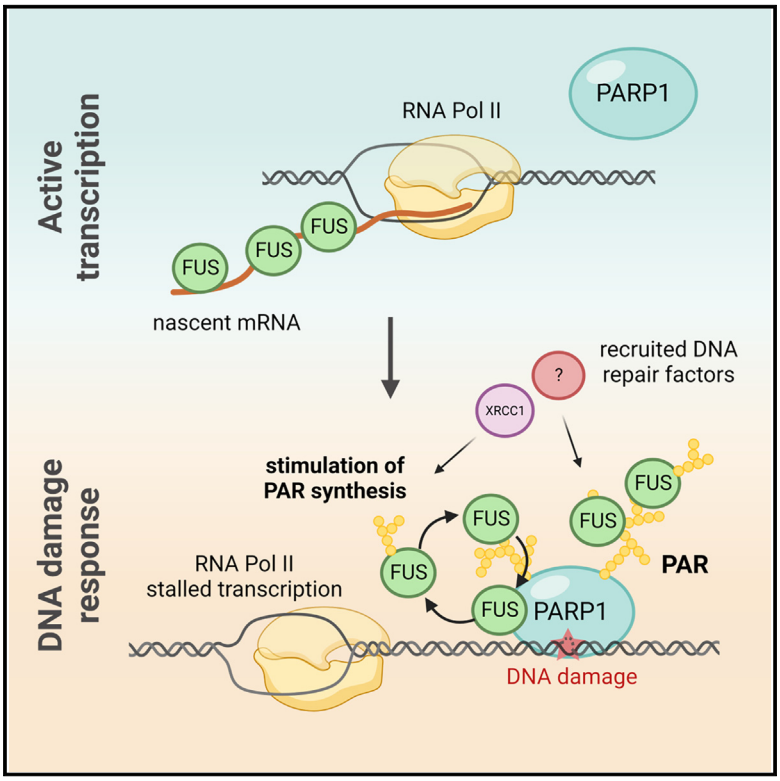

Highlights

- FUS binds specifically to PAR synthesized by PARP-1 via its RRM domain
- The recruitment of FUS to damaged DNA by PARP-1 increases nuclear PAR levels in cells
- Transcription arrest releases FUS from nascent mRNA to increase PAR level after DNA damage
- FUS is PARylated in its RRM, which possibly provides another layer of DNA repair regulation

Authors

Evgeniya M. Mamontova, Marie-Jeanne Clément, Maria V. Sukhanova, ..., Loic Hamon, Olga I. Lavrik, David Pastré

Correspondence

lavrik@niboch.nsc.ru (O.I.L.), david.pastre@univ-evry.fr (D.P.)

In brief

Mamontova et al. investigate the role of FUS in PARP-1-mediated DNA repair. They find that FUS increases nuclear PAR level upon genotoxic stress due to the specific recognition of PAR by the FUS RRM. The increase of PAR level is promoted by transcription arrest, which releases FUS from nascent mRNAs.

Mamontova et al., 2023, Cell Reports *42*, 113199
October 31, 2023
https://doi.org/10.1016/j.celrep.2023.113199

CellPress

Cell Reports

CellPress
OPEN ACCESS

Article

FUS RRM regulates poly(ADP-ribose) levels after transcriptional arrest and PARP-1 activation on DNA damage

Evgeniya M. Mamontova,[1,2,3] Marie-Jeanne Clément,[1,4] Maria V. Sukhanova,[2,4] Vandana Joshi,[1] Ahmed Bouhss,[1] Juan Carlos Rengifo-Gonzalez,[1] Bénédicte Desforges,[1] Loic Hamon,[1] Olga I. Lavrik,[2,3,*] and David Pastré[1,5,*]

[1]SABNP, University Evry, INSERM U1204, Université Paris-Saclay, 91025 Evry, France
[2]Institute of Chemical Biology and Fundamental Medicine SB RAS, Lavrentiev Av. 8, Novosibirsk 630090, Russia
[3]Department of Natural Sciences, Novosibirsk State University, 2 Pirogov Street, Novosibirsk 630090, Russia
[4]These authors contributed equally
[5]Lead contact
*Correspondence: lavrik@niboch.nsc.ru (O.I.L.), david.pastre@univ-evry.fr (D.P.)
https://doi.org/10.1016/j.celrep.2023.113199

SUMMARY

PARP-1 activation at DNA damage sites leads to the synthesis of long poly(ADP-ribose) (PAR) chains, which serve as a signal for DNA repair. Here we show that FUS, an RNA-binding protein, is specifically directed to PAR through its RNA recognition motif (RRM) to increase PAR synthesis by PARP-1 in HeLa cells after genotoxic stress. Using a structural approach, we also identify specific residues located in the FUS RRM, which can be PARylated by PARP-1 to control the level of PAR synthesis. Based on the results of this work, we propose a model in which, following a transcriptional arrest that releases FUS from nascent mRNA, FUS can be recruited by PARP-1 activated by DNA damage to stimulate PAR synthesis. We anticipate that this model offers new perspectives to understand the role of FET proteins in cancers and in certain neurodegenerative diseases such as amyotrophic lateral sclerosis.

INTRODUCTION

In cells, DNA insults need to be fixed continuously.[1,2] In the case of single-strand breaks, two abundant enzymes of the PARP family, PARP-1 and PARP-2, quickly recognize DNA damage sites. Within seconds, once positioned on DNA breaks, PARP-1 and PARP-2 synthesize poly(ADP-ribose) (PAR) using NAD^+ as a substrate. PARP-1 and, to a lesser extent, PARP-2 account for most of the PAR synthesis in the nucleus. PAR is a long, negatively charged sugar-phosphate chain covalently attached to an acceptor protein.[3,4] Acceptor proteins include PARP-1 itself, histones, DNA repair factors, or other proteins located in the vicinity of the PARP catalytic domain. Many roles have been attributed to PAR, such as opening the chromatin by displacing histones to facilitate DNA repair[5,6] and recruiting DNA repair factors.[7,8] Long PAR chains have a very short life, from seconds to minutes, because poly(ADP-ribose) glycohydrolase (PARG) rapidly hydrolyzes PAR.[3] The hydrolysis of PAR is important to release DNA repair factors after DNA damage repair.

During PARP-1 activation, many recruited protein factors have already been identified from large-scale analyses. Either their affinity for PAR (PAR reader)[9] or their PARylation (PAR acceptor)[10–13] has been used for this purpose. The identified proteins include DNA repair factors such as XRCC1, whose PAR binding domain is known,[14] but also proteins whose link with DNA repair is less clear. Among them, RNA-binding proteins (RBPs) provide a possible link between transcription and DNA repair when DNA damages halt mRNA transcriptions.[15] Some RBPs interact with RNA polymerase II[16,17] to potentially regulate the transcription status. RNA-binding proteins also have the ability to form liquid-like condensates via their low-complexity domains.[18,19] Therefore, RBPs could stimulate the compartmentalization of DNA repair sites to allow the recruitment of DNA repair factors. In addition, RBPs can also recruit RNA, notably non-coding RNA, which may also play a role in DNA repair.[20,21]

In this context, the role of many RBPs in DNA repair has already been investigated, such as for TDP-43,[22] FUS,[23–26] HuR,[27] and NONO.[28] However, if we consider PARP-dependent DNA repair, members of the FET family, FUS, TAF15, and EWSR1, occupy a central position. FET proteins were repeatedly identified in independent large-scale analyses of PARylated proteins.[10,12] They are also rapidly recruited at DNA damage sites after laser beam damage.[29,30] Accordingly, FET proteins were identified as PAR readers.[31,32] Such accumulation of experimental evidence is not shared by most RBPs, such as TDP-43, HuR, and NONO. The present study is centered on FUS, which has an even closer link with neurodegenerative diseases than TAF-15 and EWSR1. Many pathological mutations were indeed identified in FUS.[33] FUS is also frequently detected in the cytoplasmic inclusions in neurons of amyotrophic lateral sclerosis (ALS) patients.[33] The interaction between FUS and PAR is mainly orchestrated by its unstructured *arginine-glycine-rich* (RGG) domains.[31,34] In addition, FUS N-terminal domain is composed of repetitive self-adhesive sequences of

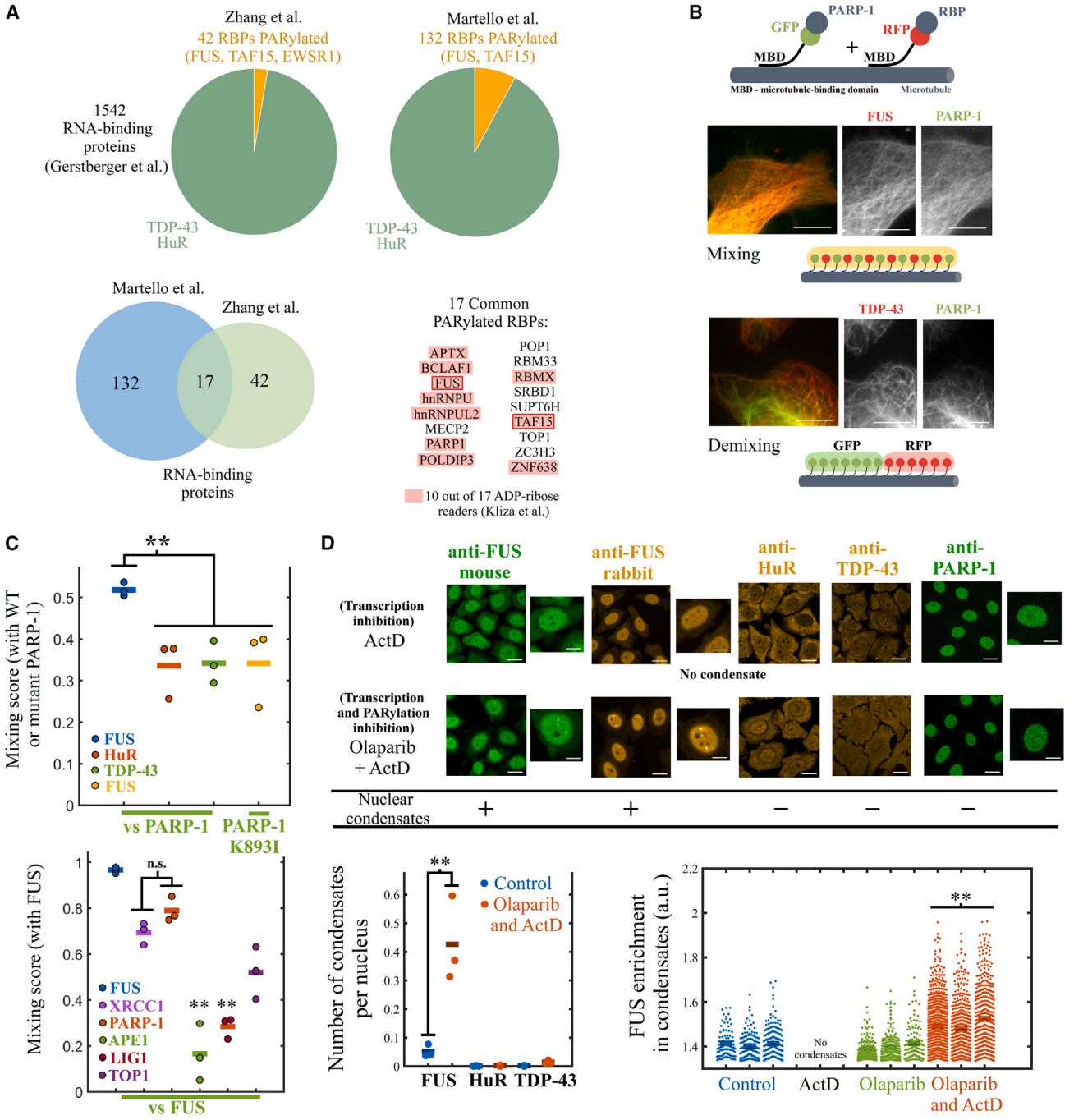

Figure 1. PARP-1 preferentially interacts and mixes with FUS in cells, and PARP-1-mediated PAR synthesis prevents aberrant FUS self-assemblies after transcription inhibition

(A) PARylation among the 1,542 known RNA-binding proteins after cell exposure to hydrogen peroxide. Upper panel: proportion of RBPs PARylated. Lower panel: overlap between the RBPs identified as PARylated from the two indicated independent studies. List of PARylated RBPs in common and PAR readers is given.

(B) Principle of the microtubule bench assay used to measure the mixing/demixing score of two different proteins. The analysis of their respective fluorescence shows a mixing of PARP-1 with FUS but not with TDP-43. MBD, microtubule-binding domain. Scale bar: 5 μm.

(C) Mixing scores for different pairs of proteins with an automated pipeline. Upper panel: mixing score of different RBP-PARP-1 wild types and RBP-PARP-1 (K893I), a PARylation-defective mutant. Lower panel: mixing score of FUS-FUS and FUS- DNA repair factors interactions. Each dot is the result of single-cell analysis in a single well (see Figure S1 for details).

(legend continued on next page)

QGSY residues. Together with the RGG domains, the QGSY domain promotes the formation of liquid-like condensates with increased efficiency in the presence of PAR[31,32,35] and RNA.[36] FUS has also been shown to be recruited to DNA damage sites after PARP-1 activation to form PARG-reversible DNA damage-enriched compartments.[37] Furthermore, the involvement of FUS in the repair of different types of DNA damage has also been largely documented.[23–26,38] Therefore, a possible link between DNA repair deregulation and neurodegenerative mechanisms was proposed.[23,39]

Several questions remain, however, unanswered about the biological functions of FUS in PARP-1-dependent DNA repair mechanisms. Hints may be found in the differences between FUS and other RBPs regarding their role in RNA processing. Interestingly, in RNA cross-linking and immunoprecipitation (CLIP) profiles, FUS but also TAF15 bind to introns with a limited sequence specificity compared, for example, to U2AF65 and TDP-43.[40,41] FUS CLIP profile also displays a typical saw-tooth pattern,[40,41] which indicates that FUS preferentially binds to nascent mRNA during transcription. As most DNA damages occur in open, transcriptionally active chromatin,[42–44] FUS can rapidly shuttle from nascent mRNAs to DNA damage sites. Another question is how FUS could interact specifically with PAR in cells. Indeed, other RBPs that bear repeats of RG-, RGG-, or SR- and KR-rich residues could bind to PAR as well as FUS.[32]

Here, using a structural approach, we demonstrated that FUS RNA recognition motif (RRM) interacts specifically with protein-free PAR. The RRM of FUS lacks several aromatic residues that generally interact with RNA bases,[45,46] which leads to its similar interaction with RNA and PAR. We also found that FUS can significantly increase the level of PARylation in HeLa cells exposed to mild concentrations of hydrogen peroxide. Hydrogen peroxide is an oxidative stress agent known to generate rapidly repairable DNA breaks, which strongly activates PARP-1.[47] In agreement with a link between transcription and DNA repair,[48,49] stalling transcription significantly increases the capacity of FUS to increase PAR level in HeLa cells exposed to hydrogen peroxide. We also show that certain FUS RRM residues previously identified as PARylated[12] control the auto-PARylation of PARP-1 *in vitro* and the level of PARP-1 activity in cells. FUS PARylation by PARP-1 may thus provide an additional layer of DNA repair regulation.

Altogether the data presented point toward the following notion. The known dynamical[50] and unspecific binding of FUS to nascent mRNA[40] allows it to be located in close proximity to open, transcriptionally active chromatin.[40] Upon DNA breaks, mRNA transcription is locally halted.[51] Then, FUS is released from nascent mRNAs to be directed to activated PARP-1 at DNA damage sites owing to its interaction with PAR regulated by its RRM. At DNA damage sites, FUS increases PAR levels, which should promote the formation of liquid-like compartments and the recruitment of additional acceptor proteins for PARylation, including FUS itself. These results provide the basis for better understanding the specific role of FET proteins in PARP-1-related DNA repair mechanisms and the role of FET proteins in cancers and neurodegenerative diseases such as ALS.

RESULTS

FUS is commonly identified as PARylated

During genotoxic stress, PARylation preferentially takes place on charged residues, Glu, Asp, Lys,[10,12] or Ser residues whose PARylation is promoted in the presence of histone PARylation factor 1 (HPF1).[52] We consider two unbiased studies that used hydrogen peroxide to activate PARP-1.[11,12] DNA damages generated by hydrogen peroxide are rapidly repaired, in contrast with dimethyl sulfate, an alkylating agent, also used to activate PARP-1 in cells.[47] Among the 1,542 proteins previously identified as partners of RNA in human cells,[53] only 17 of them were detected to be PARylated in the two large-scale studies considered here[11,12] (Figure 1A; Table S2). Out of these 17 proteins, there are two FET proteins, TAF15 and FUS. Since many PARylated proteins are themselves PAR readers, it is not surprising that a large majority of the PARylated RBPs are considered as PAR readers (13 out of 17), including TAF15 and FUS. In addition to their presence in this short list of RBPs interacting with PARP-1, FUS is one of the first proteins to be recruited via PARP-1 activation at DNA damage sites.[25,30]

FUS interacts with PARylated PARP-1 in cells

In view of the link between FUS and PARP-1, we explored the probability of formation of compartments in which PARP-1 and FUS would be mixed. For this, we used the microtubule bench assay.[54,55] Briefly, two different RFP- or GFP-labeled proteins are brought onto microtubules thanks to a fusion with a microtubule-binding domain (MBD). Their mixing score is then measured by automatically recording the relative fluorescence of the two proteins along the microtubules with an automatic high-content screening (HCS) imager operating in confocal mode at high resolution to obtain robust data (Figures 1B, S1A, and S1B). When RBPs are confined along microtubules, they can form compartments through their self-adhesive low-complexity domains but also through mRNA, which can be used as scaffold for higher-order assemblies of RBPs.[54] Our results obtained by confining PARP-1 and different RBPs (FUS, TAF15, EWSR1, SAM68, TDP-43, HuR, G3BP1) on microtubules show that PARP-1 mixes much better with FUS than with TDP-43 and HuR, two other RBPs that are not listed as particularly PARylated proteins (Figures 1C, S1C, and S2B). In fact, all three FET proteins mix pretty well with PARP-1 compared to non-FET RBPs, most probably, because PARP-1 is activated on microtubules. It has already been shown that PARP-1 can be activated by nuclear

(D) Upper panel: representative immunofluorescence images of HeLa cells and nuclear distribution of FUS, TDP-43, HuR, and PARP-1 after transcription inhibition (ActD, 5 μg/mL, 1 h) and/or PARP-1 inhibition (olaparib, 2 μM, 1 h). mRNA was not detected in FUS condensates (Figure S4A). Zoom in on the nucleus shows the presence of FUS condensates after simultaneous inhibition of transcription and PARP-1 activity. Scale bars: 20 μm and 8 μm. Lower panel: quantification of the number of condensates per nucleus or FUS enrichment in nuclear condensates versus nucleoplasm automatically detected with antibodies raised against indicated proteins and under indicated conditions. **$p < 0.01$, paired t test; n.s., non-significant.

small nucleolar RNA [56] *in vivo* and RNA oligonucleotides *in vitro*.[57] We then devised that it may also be the case with cytoplasmic RNA. In agreement with this hypothesis, we detected the presence of PAR on microtubules when PARP-1 is brought onto microtubules but not in control cells (Figure S1D). Furthermore, a PARylation-defective PARP-1 mutant (K893I) poorly mixes with FUS in contrast with wild-type PARP-1 (Figure 1C). To further probe the relevance of our results, we also measured the mixing of FUS with itself, PARP-1, and other DNA repair factors, including apurinic/apyrimidinic endonuclease 1 (APE1), DNA ligase 1 (LIG1), X-ray repair cross complementing 1 (XRCC1), and DNA topoisomerase I (TOP1). The results of the microtubule bench assay show a strong mixing of FUS with itself but also with PARP-1 and XRCC1 (Figures 1C, S1C, and S2A). On the other hand, a marked demixing was observed with APE1, LIG1, and TOP1. FUS, therefore, seems to have a particular miscibility for PARP-1 but also XRCC1, in keeping with the reported interaction between XRCC1 and FUS.[24]

To obtain cellular data independently of the microtubule bench assay, we tested PARP-1-FUS interaction by measuring the colocalization between endogenous PARP-1 and FUS in the nucleus using a PLA assay (proximity ligation assay; Figure S3A). Our results indicate that FUS and PARP-1 are close to each other in the nucleus. The occurrence of this spatial proximity is, however, more pronounced when cells are treated with H_2O_2 to activate PARP-1. As cell pretreatment with olaparib, a PARP-1 inhibitor, together with H_2O_2 (Figure S3A) significantly decreases the colocalization between PARP-1 and FUS, we infer that PARP-1 and FUS are in close proximity thanks to PAR synthesized by PARP-1. We also noticed that PARP-1 interacts with FUS even in the absence of oxidative stress, which could be due to basal PARylation of PARP-1 under physiological conditions.[58]

PAR prevents aberrant FUS self-assemblies in the nucleus after transcription inhibition

RNA is a major factor in limiting the aberrant formation of liquid phases of FUS in the nucleus.[19] We then inhibited transcription with actinomycin D (ActD) for 1 h to release FUS from nascent mRNA but observed no visible changes. Endogenous FUS remained homogeneously distributed (Figure 1D). We then also inhibited the synthesis of PAR by PARP-1 with olaparib. While olaparib alone does not generate any change in the spatial distribution of FUS, the simultaneous inhibition of PARylation and transcription generates the appearance of FUS-rich nuclear granules. The same results were obtained with two different anti-FUS antibodies (Figure 1D). In addition, the presence of similar granules was not observed with TDP-43 and HuR. In agreement with the dissociation of FUS from nascent mRNAs after transcription inhibition, mRNA was not present in the FUS granules (Figure S4A). The formation of FUS nuclear granules could therefore result from the presence of mRNA- and PAR-free FUS.

HA-FUS expression increases the PAR level in H_2O_2-treated cells in a transcription-dependent manner

Since there is a specific link between FUS and PARP-1 (Figures 1C and 1D), we then asked whether FUS may regulate PARP-1 activity in response to genotoxic stress. The point is that PAR readers are also potent acceptor proteins themselves. We devised that the presence of acceptor proteins may control the PAR level in cells.[59] To address this point, HeLa cells treated with siNeg or FUS siRNA (siFUS) were exposed to H_2O_2 for 15 min. This short-time exposure is sufficient to generate PAR synthesis in cells (Figure 2A). Using an HCS imager, we indeed detected a significant increase of PAR levels in the nuclei of H_2O_2-treated cells (Figure 2A). In addition, nuclear PAR synthesis no longer increased when HeLa cells were treated with H_2O_2 and a PARP inhibitor, olaparib. However, no difference in the overall PAR level was detected by comparing siFUS- with siNeg-treated in cells exposed to H_2O_2 (Figures 2A, S4B, and S4D). We suggested that compensatory regulation among FET proteins may hinder the putative role of FUS in regulating PARP-1 activity.

Indeed, reducing the expression of FUS changes the expression of other RBPs, notably TAF15,[41,60] which potentially can substitute FUS in the network of proteins interacting with PARP-1 (Figure 1A). As we cannot silence the expression of all FET proteins without dramatically interfering with cellular functions, we decided to overexpress HA-tagged FUS in HeLa cells. Interestingly, a significant increase in nuclear PAR level was detected in HA-FUS-expressing cells treated with H_2O_2 (Figure 2C). This pattern was not detected in HA-HuR- or HA-TDP-43-expressing cells and with the same window of nuclear HA expression at the single-cell level (Figures 2B and 2C), the nuclear overexpression of HA-RBP corresponds in average to that of endogenous FUS in the cell selected for the analysis (Figure S4C). An increased PAR level in HA-FUS-expressing cells is also observed at different time points after H_2O_2 treatment (Figure S5C). Importantly, when transcription is blocked with ActD, the level of nuclear PAR increases significantly in HeLa cells expressing HA-FUS but not HA-HuR or HA-TDP-43 (Figures 2B and 2C). In addition, the relative increase of PAR level in HA-FUS-expressing cells is more significant with 100 μM than with 300 μM of H_2O_2 (Figures 2C, S5A and S5B). FUS thus better contributes to PAR levels when DNA is not too extensively damaged. Finally, we observed that cells expressing HA-FUS, as well as control cells, do not display increased levels of DNA damages (Figure S5D).

Inhibiting mRNA transcription increases PAR level in HA-FUS-expressing cells

To better understand the mechanism behind the dramatic increase of nuclear PAR level in HA-FUS-expressing cells under ActD/H_2O_2 treatment (Figure 2C), we measured PAR levels after different times of ActD pretreatments (Figure S6). The increase of PAR level is more pronounced when HA-FUS-expressing cells were treated for at least 45 min with ActD before H_2O_2, which may correspond to the time required for releasing FUS from its mRNA targets after transcription inhibition (Figures S6A and S6C). Consistently, the nucleocytoplasmic shuttling of mRNA-binding proteins such as FUS, TDP-43, and HuR, which relies on their binding to nuclear mRNAs,[61] occurs after ActD treatment (Figure S6B).

To explore the link between RNA transcription and PAR synthesis in HA-FUS-expressing cells, we detected the incorporation of 5-bromouridine (BrU) into RNA at the single-cell level. We found that the concentrations of H_2O_2 (100–300 μM) indeed

CellPress
OPEN ACCESS

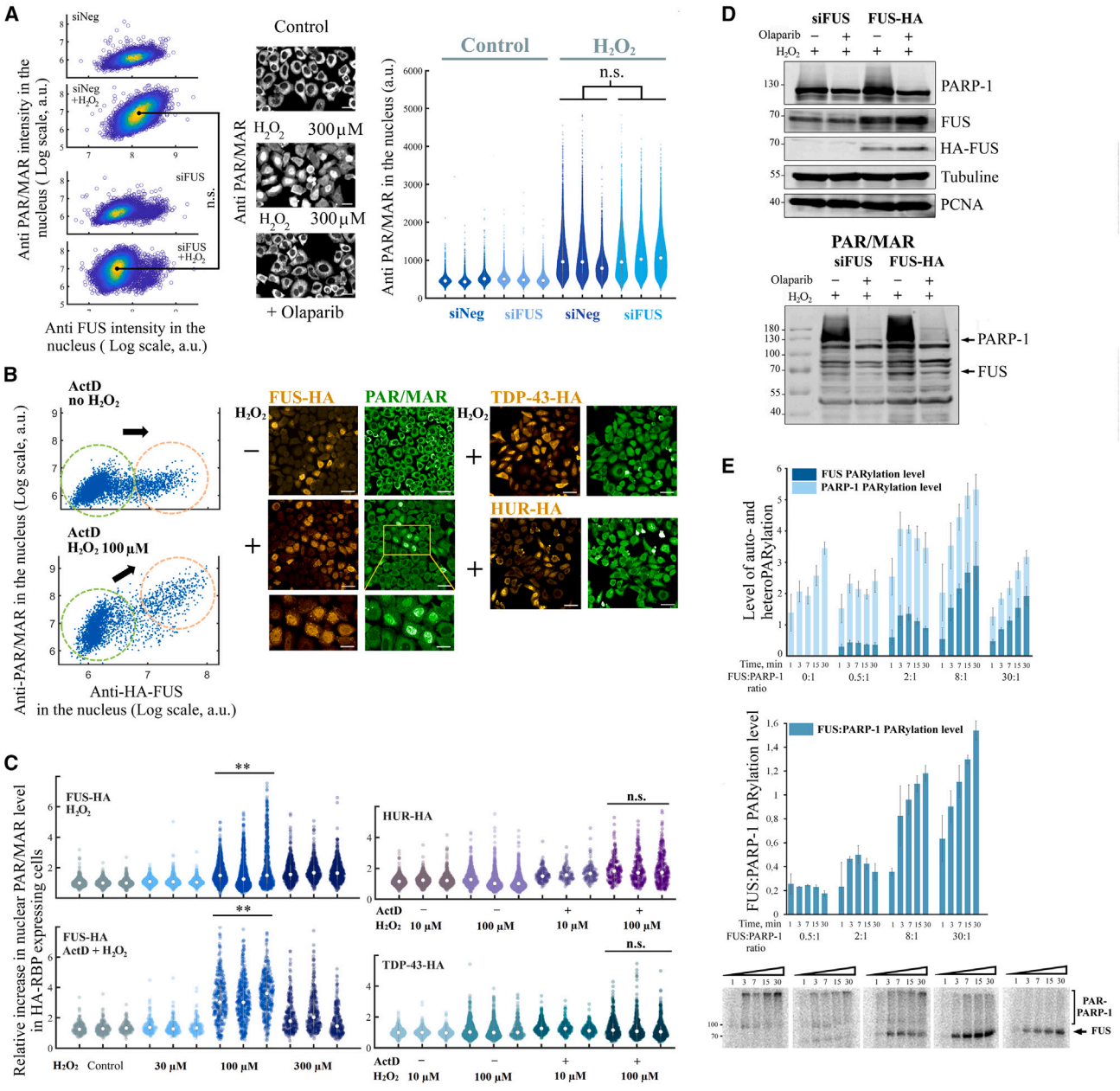

Figure 2. Overexpression of FUS increases nuclear PAR level, and recombinant FUS is highly PARylated by PARP-1 *in vitro*

(A) Left panel: scatterplot showing the level of nuclear PAR synthesis versus FUS expression level at the single-cell level in control and HeLa cells transfected with siFUS without or with H_2O_2treatment (300 μM, 15 min). Middle panel: representative immunofluorescence images under indicated treatments and antibodies. Scale bar: 25 μm. Right panel: violin plots representing the relative increase in nuclear PAR synthesis in control and cells transfected with siFUS under indicated treatment conditions. n.s., non-significant.

(B) Left panel: nuclear PAR level expressing HA-FUS treated with actinomycin D (ActD, 5 μg/mL, 1 h) or ActD and then H_2O_2 (100 μM, 30 min). Right panel: representative immunofluorescence images of cells expressing HA-tagged FUS, TDP-43, or HuR and exposed to ActD and H_2O_2 with anti-PAR/MAR and anti-HA antibodies. Scale bars: 25 μm or 50 μm.

(C) The relative increase in nuclear PAR level expressing HA-RBP versus control cells under indicated treatment conditions.

(D) Western blot analyses of protein PARylation of free fractions obtained from HEK293 cells transfected with siFUS or overexpressing HA-FUS and exposed to H_2O_2 (200 μM, 30 min) in the absence or presence of olaparib (2 μM, 1 h). Upper gel: antibodies for HA-tag and indicated proteins were used. Lower gel: antibodies to PAR/MAR were used. Note the overall increase in PAR level in HA-FUS-expressing cells.

(E) Upper panels: kinetics of PARP-1 and FUS PARylation *in vitro* at different FUS:PARP-1 concentration ratios. The overall PARylation levels of PARP-1 and FUS (upper panel) and FUS/PARP-1 PARylation ratio (lower panel) were measured from the bands presented on the gels (Figure S15.) The histogram presents the means ± SD of three independent experiments. Lower panel: PARP-1 auto-PARylation and FUS *trans*-PARylation detected by SDS-PAGE and subsequent phosphorimaging. Increasing FUS:PARP-1 ratios from left to right (see Figures S14 and S15 for details).

progressively decrease but do not totally suppress transcription in cells (Figure S7B). In addition, moderate H_2O_2 concentrations ($\leq$300 μM) did not cause major cell death (Figure S7A).

As ActD blocks both RNA polymerase I and II at the concentrations used in our experiments, we repeated the same experiments with 5,6-dichloro-1-beta-D-ribofuranosylbenzimidazole (DRB), an inhibitor of the phosphorylation of P-TEFb that promotes mRNA transcription elongation,[62] and oxaliplatin, an inhibitor of rRNA transcription. DRB, but not oxaliplatin, successfully increased the level of PAR in HA-FUS-expressing cells (Figures S8A and S8B).

We, therefore, conclude that expressing HA-FUS and inhibiting mRNA transcription significantly increase the nuclear PAR level in ActD/H_2O_2-treated cells.

FUS is significantly PARylated in cells

Given the significant increase in PAR level observed in HA-FUS-expressing cells, we asked whether FUS is PARylated and alters the level of PAR synthesis in cells. To this end, we detected the PARylation of proteins in HEK293 cells exposed to H_2O_2 in the presence or absence of olaparib to prevent PARP-1 activation (Figures S9A and S9B). In agreement with the recruitment and activation of PARP-1 at DNA damage sites, using an anti-PAR/MAR antibody, we observed in the chromatin-bound fraction a band that corresponds to PARylated PARP-1. In addition, we also noticed a band that could correspond to endogenous PARylated FUS because of its increased intensity in the absence of olaparib. A similar band was not observed for TDP-43 and HuR (Figure S9B). To ensure that this band corresponds to PARylated FUS, we expressed HA-FUS or silenced the expression of endogenous FUS to induce a measurable difference in FUS expression level. In nuclear cell extracts, we noticed an increased intensity of the band corresponding to PARylated FUS in HA-FUS-expressing cells compared to siRNA-treated cells (Figure 2D). Thus, FUS PARylation level correlates with FUS expression level. The ease with which we detected FUS PARylation from cell extracts may indicate that FUS PARylation is significant. However, FUS PARylation only represents a small fraction of the overall PARylation level (Figure 2D). Of note, we also noticed a slightly larger fraction of FUS detected in the chromatin-bound fraction in the absence than in the presence of olaparib, which indicates that PARP-1 activation may at least partly direct FUS onto chromatin (Figure S9A).

FUS enhances PARylation *in vitro* by serving as a PAR acceptor protein

Having shown an increase in PAR level observed in HA-FUS-expressing cells, we wondered what mechanism could be responsible for such an increase. An increased PAR level could be due to (1) an increased catalytic activity of PARP-1 in the presence of FUS, (2) FUS or other proteins attracted by FUS can serve as acceptor proteins, or (3) PARG activity that hydrolyzes PAR can be inhibited through the binding of FUS to PAR. To address this issue, we considered whether FUS can be PARylated and whether FUS can also stimulate PARylation in a reconstituted system in the absence of PARG. Using recombinant PARP-1 and damaged DNA, we first controlled that PARP-1 auto-PARylation increased with time in the absence of FUS (Figure 2E). In the presence of FUS up to a FUS:PARP-1 molar ratio of 8:1, the overall PARylation rate steadily increases, and then it decreases for the highest ratio of 30:1 (Figure 2E). Importantly, FUS is itself significantly PARylated by PARP-1, which accounts for most of the increase in PAR level. Therefore, FUS is an acceptor protein, which increases the number of additional targets on which PAR can be attached, but it does not significantly increase PARP-1 auto-PARylation. Finally, in a previous study, FUS did not significantly inhibit PAR hydrolysis compared to other RBPs that do not interact *in vitro* with PAR, such as HuR.[37]

Structural basis of the recognition of PAR by FUS RRM

Since FUS promotes PAR synthesis in cells and is effectively PARylated *in vitro* (Figures 2C and 2E), we focus our attention on the molecular interaction between PARP-1 and FUS. PAR is a long chain resembling RNA but with two phosphate groups in between consecutive bases instead of one for RNA. PAR is thus highly negatively charged, which may explain the affinity of arginine-rich domains for PAR. Most previous studies indicate that FUS RGG domains, notably those located in the C terminus domain of FUS, are responsible for the high affinity of FUS for PAR.[31,34] However, repeats of RG, RGG, or SR domains are quite abundant in many different RBPs.[63,64] Therefore, we wondered whether a structured domain might secure the specificity of FUS toward PAR in cells. RNA-binding domains and notably RRMs have already been proposed as PAR readers for several RBPs such as NONO.[28] Interestingly, among the 17 RBPs that were previously identified as PARylated in two independent studies[11,12] (Figure 1A), only FUS and TAF15 have PARylated residues located in their RRM domain. In addition, in the study of Zhang et al.,[12] the three FET proteins RRMs, TAF15, EWSR1, and FUS, were PARylated in two conserved negative residues, Asp-Asp or Asp-Glu, located in the short loop connecting β3 and β4 sheets (Figure 3A). This analysis thus also indicates a putative PARylation of the RRM of FET proteins.

To document whether FUS RRM specifically interacts with PAR, we first compared the amino acid sequences of FET protein RRMs with sequences of canonical RRMs of non-FET proteins like HuR, TDP-43, RMB-45, and MSI-1 (Figure 3A). One discrepancy is the presence of a long Lys-Lys loop (KK loop) in between β1(RNP2) and β2(RNP3) sheets. In addition, FUS RRM has a non-canonical β3(RNP1) sheet, an amino acid sequence involved in the binding to RNA. There are no aromatic residues in the RNP1 motif of FET proteins.[45,46] In contrast, canonical RNP1 of most RBPs has some aromatic residues, Y or F, to initiate stacking interactions with RNA bases (Figure 3A). Then, we observed the chemical shift perturbations (CSPs) of the RRM residues in the presence of protein-free PAR (Figure S10). In the presence of PAR, we noticed significant CSPs in the three RNP motifs and in the KK loop of FUS RRM. Under the same condition, PAR interacts with HuR RRM1 weakly and induces limited CSPs with TDP-43 RRM2 (Figures 3B and 3C; we had solubility issues with TDP-43 RRM1). Therefore, FUS RRM interacts more strongly with PAR than TDP-43 and HuR RRM. The binding of PAR to FUS RRM is very similar to that of a structured RNA loop (hnRNP RNA loop; key resources table) known to bind to FUS with a high affinity,[46] as most of the

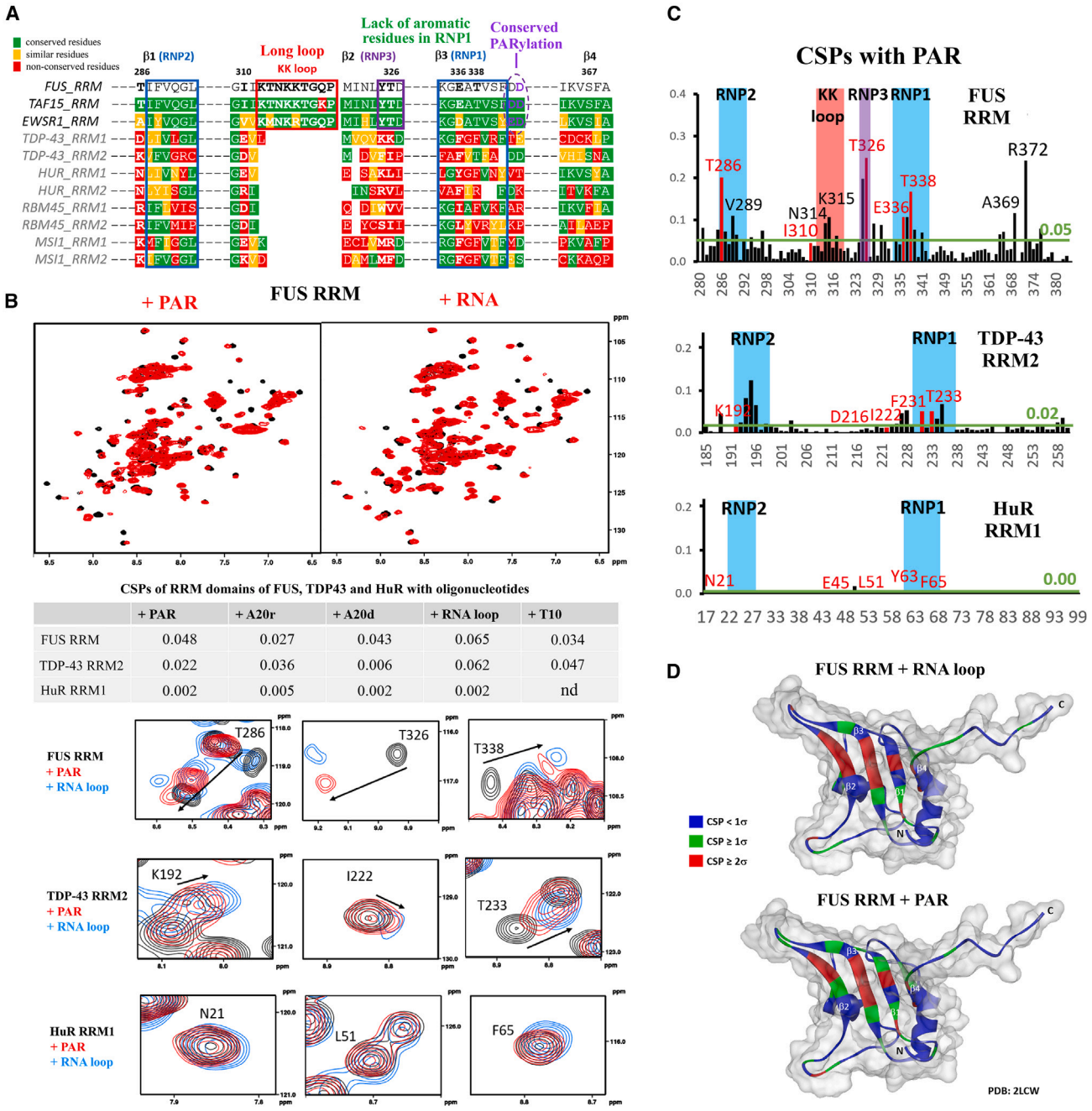

Figure 3. Structural basis of the interaction of FUS RRM with PAR, RNA, and DNA

(A) Sequence alignment of different RRMs of human RBPs. We noticed a lack of aromatic residues in RNP1and a long KK loop in FET proteins. The colors indicate a decreasing degree of conservation from green to red.

(B) Upper panel: 2D NMR spectra of the ^{15}N-labeled FUS RRM residues in the apo state (black) and in the presence of PAR or RNA loop (hnRNP RNA loop) with a FUS:RNA or DNA molar ratio of 1:1.8. Abscissa and ordinate: 1H and 15N chemical shift (in ppm), respectively. Middle panel: standard deviation of the CSP values of RBP RRM residues in the presence of indicated ligands (see also Figures S10 and S11). A20r and A20d correspond to 20 nt-long poly(A) RNA and DNA, respectively. Lower panel: zoom in on CSPs of selected RRM residues to show the similar mode of interaction of FUS RRM with PAR and RNA.

(C) Histograms displaying the CSPs of the indicated RRM residues for FUS RRM, HuR RRM1, and TDP-43 RRM2 in the presence of PAR compared to FUS RRM, HuR RRM1, and TDP-43 RRM2 alone. Note the significant CSPs observed with FUS RRM. A20r and A20d: 10-nt-long poly(A) RNA and DNA. T10, 10-nt-long poly(T) DNA.

(D) FUS RRM structure (PDB: http://doi.org/10.2210/pdb2LCW/pdb) in which the CSPs in presence of hnRNP RNA loop and PAR are indicated by colors according to their amplitude (σ of the CSP values). A similar CSP pattern is observed when FUS RRM interacts with RNA or PAR. Note the same CSP signatures when FUS RRM interacts with RNA or PAR.

CSPs occurred in the very same residues (Figures 3B and 3D). In summary, the results indicate a similar mode of binding of FUS RRM to PAR and RNA.

We then compared the binding of FUS RRM, TDP-43 RRM2, and HuR RRM1 to unstructured 20-nt-long poly(A) RNA (A20r) or poly(dA) DNA (A20d), 10-nt-long poly(T) DNA (T10), and the structured RNA (hnRNAP RNA loop) (key resources table). Poly(A) nucleotides are structurally closer to linear poly(ADP-ribose) than structured RNA (Figure S9C). Again, on average, PAR induces stronger CSPs in the RRM of FUS than of TDP-43 and HuR. In contrast, TDP-43 RRM2 interacts more with A20r and T10 than the other RRMs tested (Figures 3B, S10A, and S10B). HuR RRM1 barely interacts with A20r, A20d and PAR. Limited CSPs were also observed for HuR RRM1 with the structured RNA, whereas FUS RRM and TDP-43 RRM2 present strong CSPs with this RNA (Figure S11). These results indicate that FUS RRM does not display a marked preference for linear polymer compared with TDP-43 RRM2, which would have explained its strong interaction with PAR.

Point mutations were then used to probe the contribution of two residues in the KK loop previously shown to reduce the affinity of FUS for RNA (K315A/K316A), one residue (N284A) in the C terminus of the RRM, which displays significant CSPs with PAR, and the two Asp residues that are PARylated in cells (D342A and D343A, Table S2). None of the mutations change the overall RRM structures except some CSPs in region around the mutations (Figure S12). Based on the analysis of the CSPs (Figures S13A and S13B), the results also indicate a significant decrease in the binding of K315A/K316A to PAR, a slight decrease for N284A, and no effect for D342A/D343A RRM mutants (Figures 4A, S13A, and S13B). It is likely that the side chains K315 and K316 may contact the phosphate backbone of PAR, as observed with RNA.[46] Therefore, the KK loop, which is only found in FET proteins, is partly responsible for the strong interaction of FUS RRM with PAR, together with the lack of aromatic residues in the RNP1 motif.

PAR interacts specifically with FUS RRM and can compete with nucleic acids for the binding to FUS RRM

Pronounced PAR-induced CSPs in FUS RRM residues may enable PAR to compete with nucleic acids for binding to FUS RRM. To test this hypothesis, we chose a 10-nt-long poly(T) DNA (T10) because T10 induces similar CSPs in TDP-43- and FUS- RRM residues (Figure 4C). However, with an equimolar mixture of PAR and T10, we noticed that the CSPs of some FUS RRM residues (T326 and K315) were very similar to those observed with PAR alone as if PAR outcompetes T10 for the binding to FUS. On the other hand, TDP-43 RRM2 CSPs rather correspond to those observed with T10 alone in the presence of a mixture of T10 and PAR. To clarify whether PAR dislodges T10 from FUS RRM, we performed a WaterLOGSY assay[65] from the ligand's side. In a mixture of PAR and T10 at equimolar concentration, we clearly detected a preferential binding of FUS RRM to PAR, while TDP-43 RRM2 mostly interacts with T10 (Figure 4B). In addition, WaterLOGSY analysis indicates a specific binding of FUS RRM to H8 and H2 atoms of ADP-ribose, which is not the case for TDP-43 RRM2. To further explore the ability of FUS to bind to PAR, we probed whether FUS prevents PAR from interacting with TDP-43 RRM2. PAR induces some CSPs in TDP-43 RRM2 residues in the absence of FUS RRM. However, the addition of an equimolar concentration of non-labeled FUS RRM dramatically reduced the CSPs induced by PAR in TDP-43 RRM2 residues (Figure 4D). Altogether, our nuclear magnetic resonance (NMR) data indicate that FUS RRM is more likely to be directed to PAR compared to other canonical RRMs.

FUS RRM is important for increasing PAR levels in H_2O_2-treated HeLa cells

To explore whether the RRM of FUS plays a specific role in the increase of PAR level in cells exposed to H_2O_2, we created a construct encoding chimeric FUS protein in which FUS RRM is replaced with the RRM1 of TDP-43 (key resources table). We preferred to use TDP-43 RRM1 rather than RRM2, which has two Asp residues located in the short loop in between β3 and β4 sheets like in FUS and TAF15 proteins. TDP-43 RRM1, like RRM2, also has the typical features of canonical RRMs with aromatic residues in RNP1 motifs and no KK loop (Figure 3A). Endogenous FUS levels were decreased to better capture the impact of the FUS RRM replacement with TDP-43 RMM on PAR level in HeLa cells treated with H_2O_2 or/and ActD. HA-tagged wild-type and mutant FUS were then expressed in HeLa cells pretreated with siRNA targeting the 5′ UTR of endogenous FUS transcripts. Importantly, the overall PAR level in nuclei was measured with anti-PAR and anti-PAR/MAR, two different antibodies that we validated under our experimental conditions (Figure 5A). In addition, we compared the PAR signal in nuclei expressing the same level of nuclear HA-tagged RBPs, whatever their capacity to translocate in the cytoplasm under our experimental conditions. The level of PAR again strongly increases in HeLa cells expressing wild-type HA-FUS when treated with H_2O_2 (Figure 5B). Replacement of FUS RRM with the RRM-1 of TDP-43 completely alleviated the increase of PAR level (Figure 5B). When TDP-43 RRM1 replaces FUS RRM in full-length FUS, FUS may be routed on other nuclear RNA rather than nascent mRNA and/or lose its ability to bind to PAR.

D343A mutation significantly decreases PAR level in H_2O_2-treated cells

To further confirm our results and scrutinize how FUS RRM may control PARP-1 activity, we tested whether specific mutations in residues located in the RRM influence PAR level in ActD/H_2O_2-treated HeLa cells (Figure 5C). We considered the mutations K315A/K316A, N284A, D342A, or D343A, whose impact on RRM interaction with PAR was already assessed by NMR spectroscopy (Figures S12 and S13). To this end, we performed add-back experiments in which endogenous FUS expression was reduced before expressing FUS mutants in HeLa cells (Figure 5C). Even if K315A/K316A and N284A mutants of FUS RRM have decreased CSPs in the presence of PAR compared to wild-type RRM (Figures S10A, S10B, and S13B), adding back the expression of these FUS mutants (K315A/K316A or N284A) in FUS siRNA-pretreated cells did not affect the PAR level. In contrast, compared to wild-type FUS, adding back FUS D343A or D342A led to significantly lower PAR levels in ActD/H_2O_2-treated cells (Figure 5C).

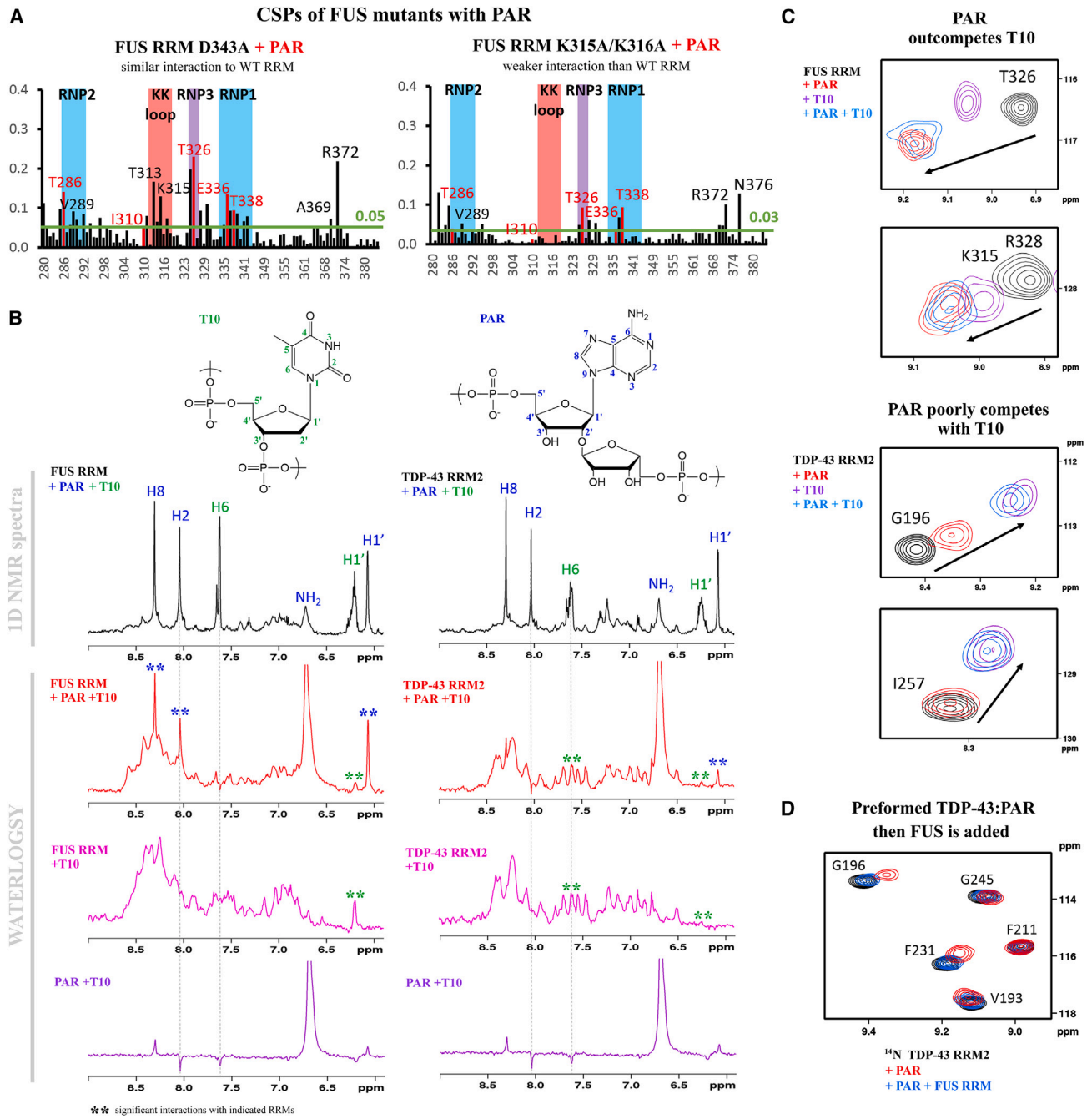

Figure 4. PAR interacts with FUS RRM and can outcompete DNA T10

(A) CSPs from NMR spectra of two FUS RRM mutants, D343A and K315A/K316A, in the presence of PAR. The FUS RRM non-conserved residues are depicted in red. Lines and numbers in green correspond to σ (standard deviation) of the CSP values.

(B) Upper panel: structural unit of PAR (*iso*-ADP-ribose motif) and T10. Lower panels: WaterLOGSY analyses of the interaction of PAR and T10, separately or in an equimolar mixture, with FUS RRM and TDP-43 RRM2. An interaction with RRM is detected when more positive ligand resonance peaks are observed in WaterLOGSY spectra in presence of RRMs compared to the spectra recorded with PAR and T10 alone. **, interactions with indicated RRMs with PAR (blue) and T10 (green). Note that PAR H8 and H2 atoms interact with FUS but not TDP-43 RRM2.

(C) NMR competition assays in the presence of PAR and/or T10 DNA for FUS RRM or TDP-43 RRM2. In specific residues, the direction or amplitudes of the CSPs varies for T10 and PAR. Zoom in on these residues indicates the preference for T10 (TDP-43 RRM2) or PAR (FUS RRM).

(D) TDP-43 RRM2 and PAR were left to interact before the addition of an equimolar concentration of unlabeled FUS RRM. The CSPs of TDP-43 are displayed for representative residues.

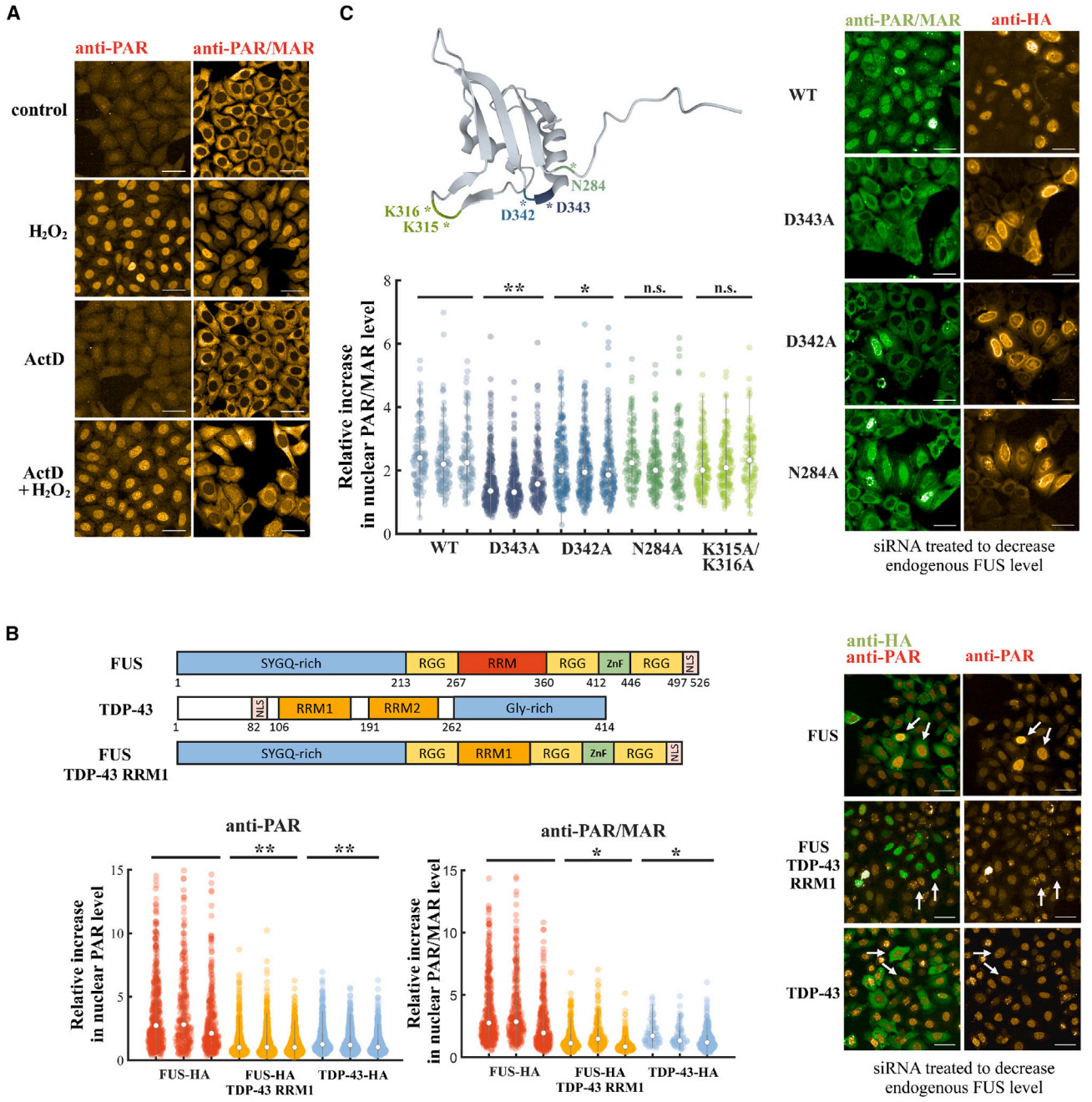

Figure 5. FUS RRM is implicated in the regulation of nuclear PAR level in ActD/H_2O_2-treated HeLa cells

(A) Immunofluorescence images of cells expressing HA-tagged FUS and treated with H_2O_2 (100 μM, 30 min), ActD (5 μg/mL, 1 h), or ActD/H_2O_2. The nuclear PAR was detected with two different antibodies. Cell treatment with ActD did not affect the PAR level (Figure S8). Scale bar: 50 μm.

(B) Upper panel: the domain structures of FUS, TDP-43, and chimeric form of FUS in which RRM is replaced with the RRM1 of TDP-43. Lower panels: violin plots representing the relative increase of nuclear PAR level in HeLa cells expressing indicated HA-tagged RBP versus control cells (left) and corresponding representative immunofluorescence images (right). The quantitative results are shown for the two different antibodies. t test versus FUS-HA expressing cells. Note the high PAR level in cells expressing FUS-HA (shown by white arrows). Scale bar: 50 μm.

(C) Upper panel: FUS RRM structure (PDB: http://doi.org/10.2210/pdb2LCW/pdb) in which the positions of N284, K315, K316, D342, and D343 residues are indicated. Lower panel: violin plots representing the relative increase of nuclear PAR level in HeLa cells treated with siFUS and expressing indicated FUS-HA mutants versus control HeLa cells. n.s., non-significant, *$p < 0.05$; **$p < 0.01$; t test versus WT FUS-HA expressing cells. Right panel: representative immunofluorescence images. Scale bar: 30 μm.

D343A mutation interferes with the interaction of FUS RRM with activated PARP-1 *in vitro*

The data obtained in cells expressing the FUS D343A mutant cannot show whether D343A directly impaired the interaction between activated PARP-1 and FUS. A doubt remains since FUS D343A RRM interaction with purified PAR and RNA is very similar to that of wild-type FUS RRM (Figures S10 and S13A). We then devised to perform an assay in which the interaction of FUS RRM with PARP-1 activated by damaged DNA can be captured by NMR spectroscopy. To this end, we first controlled that PARP-1 consumption of NAD^+ upon its activation by damaged DNA can be followed by NMR spectroscopy using recombinant PARP-1 and DNA duplexes (30 bp) containing one nucleotide gap. After the addition of DNA duplex, the synthesis of poly(ADP-ribose) was clearly evidenced in 1D NMR spectra through the progressive decrease in NAD^+ proton intensities and the increase of those of nicotinamide with time (Figure 6A). Then, we analyzed NMR spectra of wild-type FUS and D343A RRM residues after PARP-1 activation by DNA duplex. Unexpectedly, we found a significant difference. D343A RRM mutant interacted strongly with activated PARP-1 with the appearance of double peaks or their disappearance, which was not observed in the same conditions with wild-type FUS RRM (Figure 6B). Residue disappearance may be consecutive to changes in the exchange dynamics between free and bound states. The presence of double peaks is rather related to a slow exchange between two different states, which may be due to the PARylation of a fraction of these RRM residues. Further analysis of the CSPs reveals the presence of many double peak residues, notably from charged residues that can be potentially PARylated, E294, K315, K316, R328, K334, and D355 (Figures 6C and 6D).

D343A increases PARP-1 auto-PARylation *in vitro*

As NMR data reveal an increased interaction of D343A RRM with activated PARP-1 (Figure 6B), we then directly measured whether D343A FUS RRM is hyper-PARylated *in vitro*. We first remarked the low PARylation level of the FUS RRM and TDP-43 RRM2 *in vitro* (Figure 6E). In contrast, the PARylation of full-length FUS is very significant but not that of full-length TDP-43 (Figure S14E). Therefore, RRM fragments could not capture the significant PARylation of full-length FUS *in vitro*, which may mostly rely on the presence of other FUS domains, such as the RGG domains. However, D343A RRM, but not wild-type FUS RRM or TDP-43 RRM2, is strongly PARylated (Figure 6E). We also note that none of the other mutations (K315A/K316A, N284A) affect the PARylation of FUS RRM except D342A, which increases PARylation level but to a lesser extent than D343A.

To document why nuclear PAR levels are reduced in FUS D343A-expressing cells compared with wild-type FUS-expressing cells (Figure 5C), we analyzed the PARylation of full-length wild-type and D343A FUS *in vitro* (Figures 6F andS14). Wild-type FUS was strongly PARylated, but PARP-1 auto-PARylation was then slightly reduced (Figures S14 and S15). In contrast, full-length mutant D343A significantly increased PARP-1 auto-PARylation level (Figures 6F , S14, and S15). Therefore, the mutation D343A may promote the release of PARP-1 from damaged DNA.

DISCUSSION

The pathway by which FUS, a nuclear mRNA-binding protein, participates in DNA repair has not yet been clearly established. FUS interacts with PAR, the polymer produced by PARP-1 after the recognition of DNA breaks.[30,34,66] The interaction of FUS with protein-free PAR, mostly with its RGG domains, promotes the formation of compartments behaving like liquid phases.[35] FUS can also form dynamic and PARG-reversible compartments in the presence of damaged DNA following PARP-1 activation, bringing this model even closer to physiological conditions.[37] Here, we show that FUS interacts in a specific way with PAR thanks to its RRM domain, which shares specific characteristics with other FET proteins, TAF15 and EWSR1. First of all, some aromatic residues that are present in RNP1 of canonical RRMs motif are absent in FUS RRM[46] (Figure 3A). Their absence contributes to the low binding specificity of FUS regarding mRNA sequences that has been observed in genome-wide CLIP data.[40] PAR resembles RNA from a structural point of view, but the bases are separated by two negatively charged phosphate groups instead of one for RNA. Therefore, the lack of aromatic residues of the RNP1 motif could explain the similar interaction of FUS with PAR and mRNA, while canonical RRMs with their aromatic residues prefer to bind to RNA. Finally, to compensate for the loss of interaction due to the missing aromatic residues, FUS harbors a long positively charged KK loop[45] to interact electrostatically with PAR or RNA (Figures 3B and 3C). The dual and competitive interactions of PAR and RNA with FUS RRM provide a rational explanation for the high occurrence of FUS in proteomic data generated to identify PARylated proteins following oxidative stress.[10,12] Of note, arginine-rich low-complexity domains in FUS have also been shown to interact with PAR with likely important functions in DNA repair. However, the presence of arginine-rich low-complexity domains, which is quite common among RBPs,[67] is not sufficient to explain FUS preference for PARylated PARP-1.

The expression of HA-FUS, but not HA-HuR or HA-TDP-43, increases the level of PAR synthesis in cells subjected to oxidative stress (Figure 2B). The most significant increase in the level of PAR is observed when transcription is stalled and when oxidative stress does not exceed a certain level (H_2O_2 < 300 μM). These two points are important. The need to stop transcription reflects a competition between the binding of FUS to nascent mRNA and PAR. However, the binding of FUS to nascent mRNA may turn into an advantage to direct FUS to PARP-1 at DNA damages. Indeed, DNA damages more likely occur in transcription-active open chromatin where there are many nascent mRNAs.[68,69] When few DNA damages take place, transcription is locally stalled,[15] which may release protein factors, such as FUS, associated with nascent mRNA near the site of DNA damages. While higher concentrations of H_2O_2 (~300 μM) allow more DNA damages and an increase in overall PAR level (Figures S5A and S5B), the capacity of FUS to increase PAR level is altered significantly. Under these conditions, many PARP-1 proteins are activated in the nucleus, which could disperse FUS proteins over a large number of DNA damage sites and prevent several FUS proteins from being directed to the same DNA damage site. Consistently with this model, we show that FUS has the

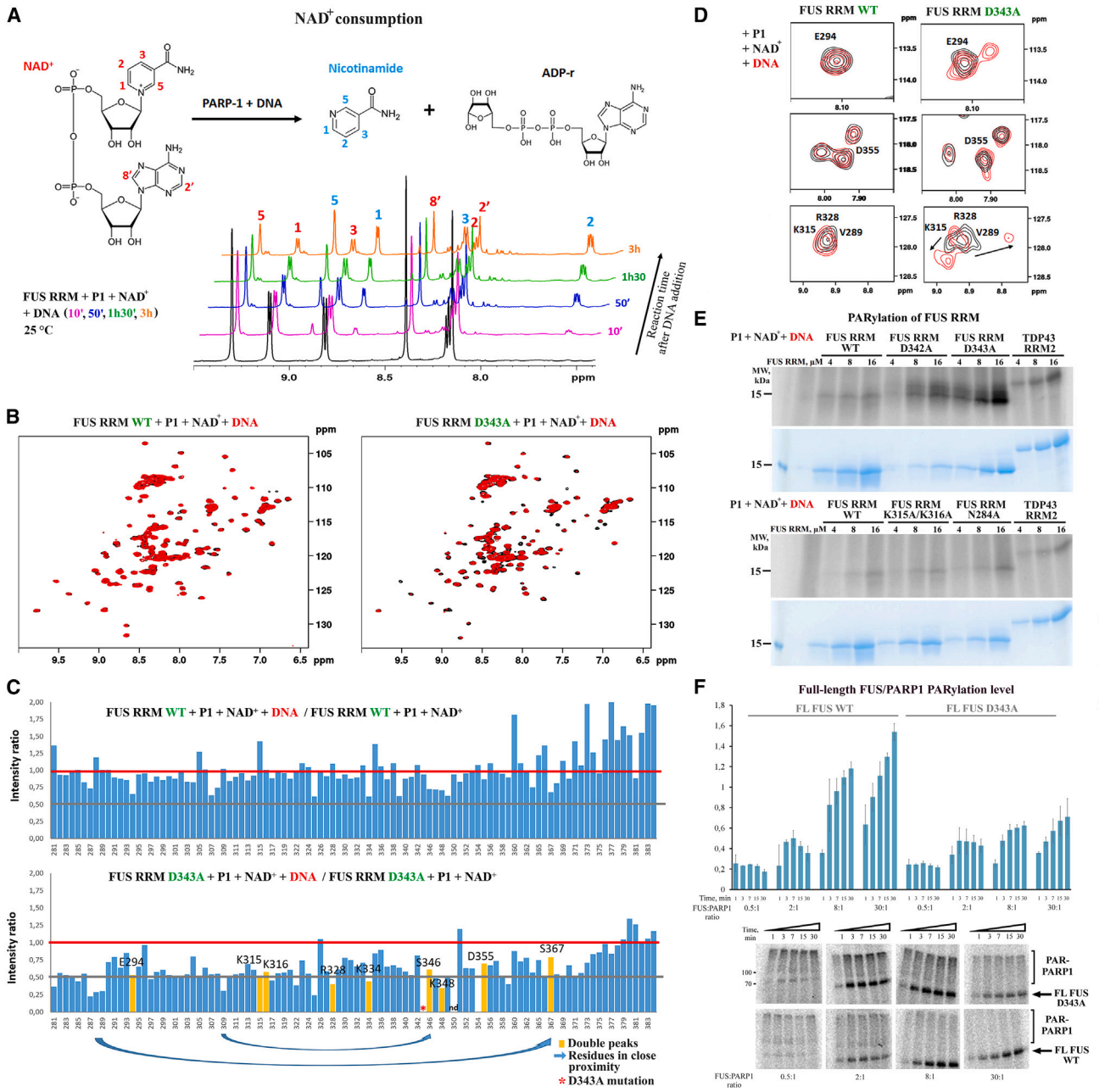

Figure 6. D343A mutation impairs the interaction of FUS RRM with PARylated PARP-1 *in vitro*

(A) 1D NMR spectra showing the gradual consumption of NAD^+ upon the activation of PARP-1 in the presence of damaged DNA. Upper: scheme of PARP-1 catalyzed reaction that leads to hydrolysis of NAD^+ to nicotinamide and ADP-ribose (ADP-r). P1 is PARP-1. NAD+ and nicotinamide signals are labeled with red and blue numbers, respectively.

(B) NMR spectra of wild-type and D343A FUS RRM in the presence (red) or absence (black) of damaged DNA to activate PARP-1. Note in the inset the broadening of some D343A RRM residues after the activation of PARP-1 but not for wild-type FUS RRM.

(C) Intensity ratio of the resonance peaks of RRM residues for wild-type and D343A FUS RRM before and after PARP-1 activation. In yellow, residues have doubling peaks. Blue arrows show residues in close proximity to disappearing/doubling peak residues. Red asterisk shows mutated residue, D343.

(D) Zoom in on several residues experiencing doubling peaks in D343A FUS RRM after PARP-1 activation.

(E) PARylation of FUS RRM WT, its indicated mutants, and TDP43 RRM2 detected by SDS-PAGE with subsequent phosphorimaging and Coomassie staining. Note the increase in the level of RRM PARylation in the case of D343A mutant and, to a lesser extent, in the case of D342A mutant.

(F) Upper panel: kinetics of PARP-1 and FUS wild type (WT) and FUS (D343A) mutant *in vitro* PARylation at different FUS:PARP-1 concentration ratios. The histogram presents the means ± SD of three independent experiments. Lower panel: PARylation of FUS WT and FUS (D343A) mutant detected by SDS-PAGE with subsequent phosphorimaging. (see Figures S14 and S15 for details).

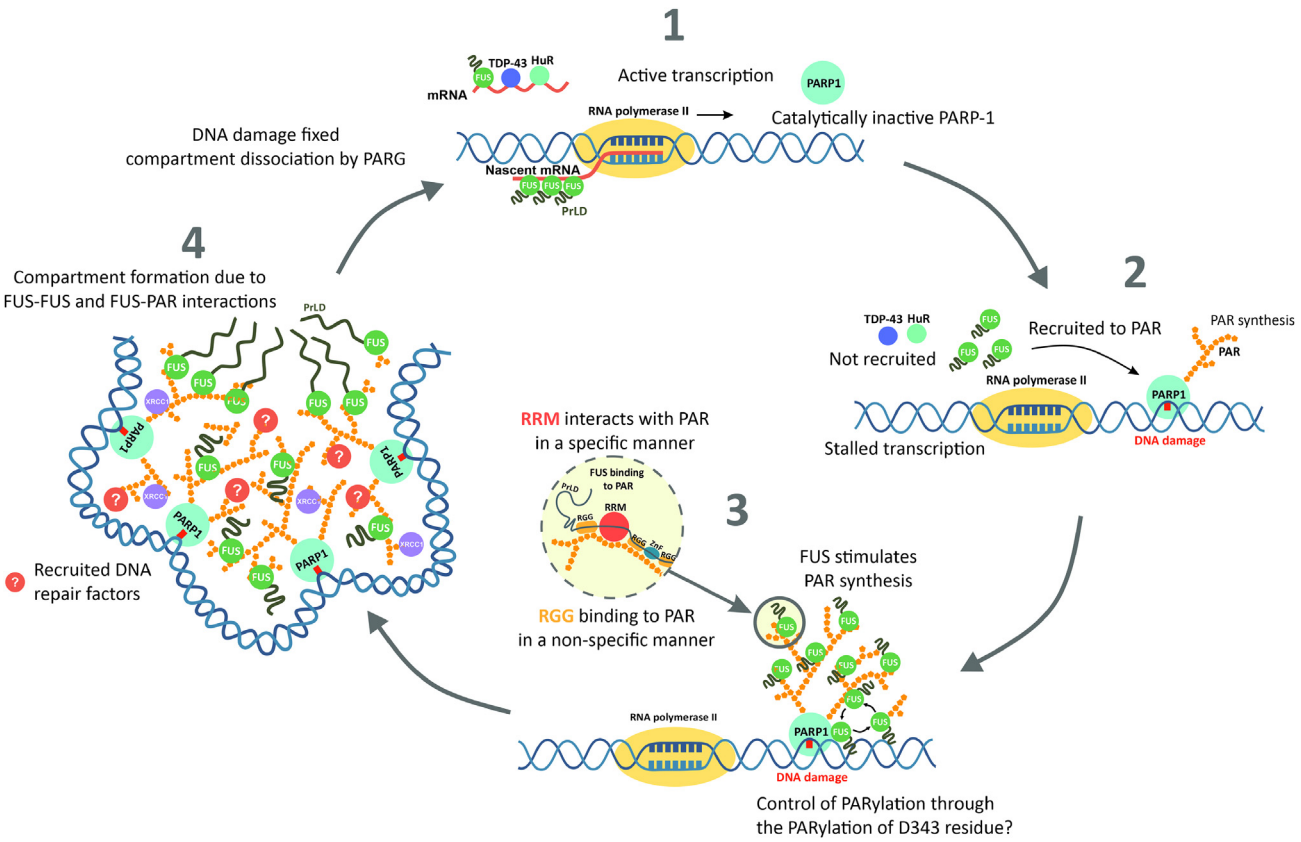

Figure 7. Schematic view of the role of FUS in PARP-1-mediated DNA repair

When RNA polymerase II transcription is taking place, FUS is bound to nascent mRNA (1). After stress, PARP-1 recognizes DNA damage to activate PAR synthesis. If transcription is also stalled, FUS is released from nascent mRNA. FUS is recruited via its RRM and RGG domains to PARylated PARP-1 (2). FUS stimulates PAR synthesis acting as PAR acceptor protein (3) and facilitates the formation of FUS-rich compartments due to FUS-FUS and FUS-PAR interactions (4). Other DNA repair factors such as XRCC1 can be recruited in these compartments (4). After DNA is repaired, the compartments are dissociated due to PAR degradation catalyzed by PARG.

ability to significantly increase the level of PARylation *in vitro* at elevated FUS:PARP-1 ratios by serving as a PAR acceptor (Figure 2E). In cells, additional protein partners are recruited in a compartment formed by FUS following the activation of PARP-1 to be themselves PARylated such as XRCC1. All these results lead us to propose the following scheme (Figure 7). After genotoxic stress, PARP-1 recognizes DNA damages, which leads to its activation and auto-PARylation. Transcription is also stalled,[15] which releases FUS from nascent mRNA in the vicinity of auto-PARylated PARP-1. FUS is then becoming a PAR acceptor to stimulate the overall rate of PARylation process, as observed *in vitro* (Figure 2E). As FUS PARylation itself cannot fully account for the increase in PAR level in cells, other proteins recruited by FUS at DNA damage sites can also serve as acceptor proteins to increase PARP-1 activity. Increasing PAR level may facilitate the formation of FUS/PAR-rich compartments enriched in DNA damage sites (Figure 7).[34,37]

In this study, we also documented the role of D343 residue previously identified as potentially PARylatable in the RRM of FET proteins.[12] D343A mutation does not change the FUS RRM structure (Figure S12). The interaction of FUS RRM with nucleic acids and protein-free PAR is also not altered (Figure S13A). However, D343A mutation drastically modifies the interaction of FUS RRM with PARP-1 following its activation by damaged DNA *in vitro* (Figures 6B and 6C). Importantly, the D343A mutation reduces the PAR level in cells overexpressing HA-FUS and exposed to ActD and H_2O_2 (Figure 5C). *In vitro*, full-length D343A increases PARP-1 auto-PARylation (Figure 6F). Since PARP-1 auto-PARylation promotes the release of PARP-1 from DNA damage, D343A may reduce PAR synthesis[70] in cells by increasing PARP-1 auto-PARylation.[4,71] These results open up the possibility that PARylation of FUS RRM may be used as another layer of regulation to control PARP-1 activation in cells. Even if we focus our attention on FUS RRM in this study, additional residues located in FUS low-complexity domains have been identified as targets of PARylation, including serine residues whose PARylation is controlled by HPF1.[12,72] Their PARylation may also play a role in the cell response to DNA damage that deserves to be investigated.

We anticipate that the result presented here will provide a basis for understanding the role of FUS in the regulation of PARP-1 activity, notably in cancers for which PARP-1 is an important target, with several FDA-approved drugs being already available for different indications.[73] Other perspectives of this work are

obviously associated with neurodegenerative diseases such as ALS in which pathological FET protein mutations have been identified.[74] We did not investigate whether pathological FUS mutations or posttranslational modifications (phosphorylation or methylation[75,76]) may interfere with the capacity of FUS to regulate PARylation, which may be interesting to address in the future. In addition, the C-terminal RG-rich domains are known to interact with PAR and to be the recipient of many pathological mutations in ALS[77] as well as posttranslational modifications,[75] whose roles within the frame of our model also deserve to be explored. Finally, the model we have proposed also highlights a possible coordination between mRNA transcription and PARP-1-related DNA repair orchestrated by FET proteins.

Limitations of the study

Our study has certain limitations. Most cellular results were obtained after overexpressing or after adding back the expression of wild-type or mutant FUS, which may not totally reflect the behavior of endogenous FUS in animals. Hydrogen peroxide has been used to activate PARP-1, thus allowing to quantify PAR level at the single-cell level. Although our work demonstrates that FUS can increase PAR levels *in vitro* and in cells after hydrogen peroxide treatment, we didn't demonstrate whether FUS could play a similar role when DNA damages are occurring locally in open chromatin.

STAR★METHODS

Detailed methods are provided in the online version of this paper and include the following:

- KEY RESOURCES TABLE
- RESOURCE AVAILABILITY
  - Lead contact
  - Materials availability
  - Data and code availability
- EXPERIMENTAL MODEL AND STUDY PARTICIPANT DETAILS
  - Cell culture
- METHOD DETAILS
  - Preparation of plasmids for expression in mammalian and E.coli cells
  - Plasmid transfection, siRNA treatment and addback experiments
  - Microtubule bench assay
  - High-content imaging assay and analysis
  - *In situ* RNA hybridization
  - 5-Bromouridin (BrU) incorporation analysis
  - Proximity ligation assay (PLA)
  - Isolation of chromatin-bound proteins and Western blot analysis
  - Recombinant protein production and purification
  - Radioactive assay of protein PARylation *in vitro*
  - NMR analysis
- QUANTIFICATION AND STATISTICAL ANALYSIS
  - Analysis of cell by HCS fluorescence microscopy
  - Analysis of the level of protein PARylation *in vitro*
  - Statistical analysis

SUPPLEMENTAL INFORMATION

Supplemental information can be found online at https://doi.org/10.1016/j.celrep.2023.113199.

ACKNOWLEDGMENTS

We are grateful to Dr. Pablo Radicella (Institute of Molecular and Cellular Radiobiology, France) for XRCC1-encoding plasmid, Dr. M. Satoh (Laval University, Canada) for PARP-1-encoding plasmid, Dr. S.H. Wilson (NIEHS, NIH, USA) for APE1-encoding plasmid, and Dr. S.I. Shram (Institute of Molecular Genetic RAS, Moscow) for providing us NMNAT.

We thank INSERM (PRI, RaPiD) and University of Evry for continuous support of the SABNP laboratory. This work was supported in part by the Région Ile-de-France (SESAME grant no. 15013102) and Genopole (SATURNE grant 2020). This study was supported by the Russian Science Foundation (RSF 22-14-00112 to O.I.L. and RSF 20-14-00086 to M.V.S.) and the International doctoral action (ADI2019) program of Paris-Saclay Université (PhD grant to E.M.M.). The graphical abstract was created with BioRender.com.

AUTHOR CONTRIBUTIONS

Conceptualization: E.M.M., L.H., M.V.S., O.I.L., and D.P.; methodology: E.M.M., M.-J.C., B.D., V.J., J.C.R.-G., and A.B.; validation: E.M.M., M.-J.C., L.H., and M.V.S.; formal analysis: E.M.M., M.-J.C., M.V.S., L.H., O.I.L., and D.P.; resources: M.-J.C., E.M.M., L.H., M.V.S., B.D., V.J., J.C.R.-G., and A.B.; data curation: E.M.M., M.V.S., and L.H.; writing – review & editing: O.I.L. and D.P.; visualization: E.M.M., M.V.S., L.H., O.I.L., and D.P.; supervision: O.I.L. and D.P.; project administration: O.I.L. and D.P.

DECLARATION OF INTERESTS

The authors declare no competing interests.

Received: March 6, 2023
Revised: July 8, 2023
Accepted: September 15, 2023
Published: October 5, 2023

REFERENCES

1. Ciccia, A., and Elledge, S.J. (2010). The DNA damage response: making it safe to play with knives. Mol. Cell *40*, 179–204. https://doi.org/10.1016/j.molcel.2010.09.019.
2. Schreiber, V., Dantzer, F., Ame, J.C., and de Murcia, G. (2006). Poly(ADP-ribose): novel functions for an old molecule. Nat. Rev. Mol. Cell Biol. *7*, 517–528. https://doi.org/10.1038/nrm1963.
3. Illuzzi, G., Fouquerel, E., Amé, J.C., Noll, A., Rehmet, K., Nasheuer, H.P., Dantzer, F., and Schreiber, V. (2014). PARG is dispensable for recovery from transient replicative stress but required to prevent detrimental accumulation of poly(ADP-ribose) upon prolonged replicative stress. Nucleic Acids Res. *42*, 7776–7792. https://doi.org/10.1093/nar/gku505.
4. Alemasova, E.E., and Lavrik, O.I. (2019). Poly (ADP-ribosyl) ation by PARP1: reaction mechanism and regulatory proteins. Nucleic Acids Res. *47*, 3811–3827.
5. Luo, X., and Kraus, W.L. (2012). On PAR with PARP: cellular stress signaling through poly (ADP-ribose) and PARP-1. Genes Dev. *26*, 417–432.
6. Ray Chaudhuri, A., and Nussenzweig, A. (2017). The multifaceted roles of PARP1 in DNA repair and chromatin remodelling. Nat. Rev. Mol. Cell Biol. *18*, 610–621.
7. Haince, J.-F., McDonald, D., Rodrigue, A., Déry, U., Masson, J.-Y., Hendzel, M.J., and Poirier, G.G. (2008). PARP1-dependent kinetics of recruitment of MRE11 and NBS1 proteins to multiple DNA damage sites. J. Biol. Chem. *283*, 1197–1208.

8. Hanzlikova, H., Gittens, W., Krejcikova, K., Zeng, Z., and Caldecott, K.W. (2017). Overlapping roles for PARP1 and PARP2 in the recruitment of endogenous XRCC1 and PNKP into oxidized chromatin. Nucleic Acids Res. *45*, 2546–2557.

9. Kliza, K.W., Liu, Q., Roosenboom, L.W.M., Jansen, P.W.T.C., Filippov, D.V., and Vermeulen, M. (2021). Reading ADP-ribosylation signaling using chemical biology and interaction proteomics. Mol. Cell *81*, 4552–4567.e8.

10. Jungmichel, S., Rosenthal, F., Altmeyer, M., Lukas, J., Hottiger, M.O., and Nielsen, M.L. (2013). Proteome-wide identification of poly (ADP-Ribosyl) ation targets in different genotoxic stress responses. Mol. Cell *52*, 272–285.

11. Martello, R., Leutert, M., Jungmichel, S., Bilan, V., Larsen, S.C., Young, C., Hottiger, M.O., and Nielsen, M.L. (2016). Proteome-wide identification of the endogenous ADP-ribosylome of mammalian cells and tissue. Nat. Commun. *7*, 12917.

12. Zhang, Y., Wang, J., Ding, M., and Yu, Y. (2013). Site-specific characterization of the Asp-and Glu-ADP-ribosylated proteome. Nat. Methods *10*, 981–984.

13. Gagné, J.P., Pic, E., Isabelle, M., Krietsch, J., Ethier, C., Paquet, E., Kelly, I., Boutin, M., Moon, K.M., Foster, L.J., and Poirier, G.G. (2012). Quantitative proteomics profiling of the poly(ADP-ribose)-related response to genotoxic stress. Nucleic Acids Res. *40*, 7788–7805. https://doi.org/10.1093/nar/gks486.

14. Breslin, C., Hornyak, P., Ridley, A., Rulten, S.L., Hanzlikova, H., Oliver, A.W., and Caldecott, K.W. (2015). The XRCC1 phosphate-binding pocket binds poly (ADP-ribose) and is required for XRCC1 function. Nucleic Acids Res. *43*, 6934–6944.

15. Gregersen, L.H., and Svejstrup, J.Q. (2018). The cellular response to transcription-blocking DNA damage. Trends Biochem. Sci. *43*, 327–341.

16. Schwartz, J.C., Ebmeier, C.C., Podell, E.R., Heimiller, J., Taatjes, D.J., and Cech, T.R. (2012). FUS binds the CTD of RNA polymerase II and regulates its phosphorylation at Ser2. Genes Dev. *26*, 2690–2695.

17. Burke, K.A., Janke, A.M., Rhine, C.L., and Fawzi, N.L. (2015). Residue-by-residue view of in vitro FUS granules that bind the C-terminal domain of RNA polymerase II. Mol. Cell *60*, 231–241.

18. Wang, J., Choi, J.-M., Holehouse, A.S., Lee, H.O., Zhang, X., Jahnel, M., Maharana, S., Lemaitre, R., Pozniakovsky, A., Drechsel, D., et al. (2018). A molecular grammar governing the driving forces for phase separation of prion-like RNA binding proteins. Cell *174*, 688–699.e16.

19. Maharana, S., Wang, J., Papadopoulos, D.K., Richter, D., Pozniakovsky, A., Poser, I., Bickle, M., Rizk, S., Guillén-Boixet, J., Franzmann, T.M., et al. (2018). RNA buffers the phase separation behavior of prion-like RNA binding proteins. Science *360*, 918–921.

20. d'Adda di Fagagna, F. (2014). A direct role for small non-coding RNAs in DNA damage response. Trends Cell Biol. *24*, 171–178.

21. Majidinia, M., and Yousefi, B. (2016). Long non-coding RNAs in cancer drug resistance development. DNA Repair *45*, 25–33.

22. Mitra, J., Guerrero, E.N., Hegde, P.M., Liachko, N.F., Wang, H., Vasquez, V., Gao, J., Pandey, A., Taylor, J.P., Kraemer, B.C., et al. (2019). Motor neuron disease-associated loss of nuclear TDP-43 is linked to DNA double-strand break repair defects. Proc. Natl. Acad. Sci. USA. *116*, 4696–4705.

23. Naumann, M., Pal, A., Goswami, A., Lojewski, X., Japtok, J., Vehlow, A., Naujock, M., Günther, R., Jin, M., Stanslowsky, N., et al. (2018). Impaired DNA damage response signaling by FUS-NLS mutations leads to neurodegeneration and FUS aggregate formation. Nat. Commun. *9*, 335.

24. Wang, H., Guo, W., Mitra, J., Hegde, P.M., Vandoorne, T., Eckelmann, B.J., Mitra, S., Tomkinson, A.E., Van Den Bosch, L., and Hegde, M.L. (2018). Mutant FUS causes DNA ligation defects to inhibit oxidative damage repair in Amyotrophic Lateral Sclerosis. Nat. Commun. *9*, 3683.

25. Levone, B.R., Lenzken, S.C., Antonaci, M., Maiser, A., Rapp, A., Conte, F., Reber, S., Mechtersheimer, J., Ronchi, A.E., Mühlemann, O., et al. (2021). FUS-dependent liquid–liquid phase separation is important for DNA repair initiation. J. Cell Biol. *220*, e202008030.

26. Wang, W.-Y., Pan, L., Su, S.C., Quinn, E.J., Sasaki, M., Jimenez, J.C., Mackenzie, I.R.A., Huang, E.J., and Tsai, L.-H. (2013). Interaction of FUS and HDAC1 regulates DNA damage response and repair in neurons. Nat. Neurosci. *16*, 1383–1391.

27. Gorospe, M. (2003). HuR in the mammalian genotoxic response: post-transcriptional multitasking. Cell Cycle *2*, 411–413.

28. Krietsch, J., Caron, M.-C., Gagné, J.P., Ethier, C., Vignard, J., Vincent, M., Rouleau, M., Hendzel, M.J., Poirier, G.G., and Masson, J.-Y. (2012). PARP activation regulates the RNA-binding protein NONO in the DNA damage response to DNA double-strand breaks. Nucleic Acids Res. *40*, 10287–10301.

29. Izhar, L., Adamson, B., Ciccia, A., Lewis, J., Pontano-Vaites, L., Leng, Y., Liang, A.C., Westbrook, T.F., Harper, J.W., and Elledge, S.J. (2015). A Systematic Analysis of Factors Localized to Damaged Chromatin Reveals PARP-Dependent Recruitment of Transcription Factors. Cell Rep. *11*, 1486–1500. https://doi.org/10.1016/j.celrep.2015.04.053.

30. Rulten, S.L., Rotheray, A., Green, R.L., Grundy, G.J., Moore, D.A.Q., Gómez-Herreros, F., Hafezparast, M., and Caldecott, K.W. (2014). PARP-1 dependent recruitment of the amyotrophic lateral sclerosis-associated protein FUS/TLS to sites of oxidative DNA damage. Nucleic Acids Res. *42*, 307–314. https://doi.org/10.1093/nar/gkt835.

31. Rhine, K., Dasovich, M., Yoniles, J., Badiee, M., Skanchy, S., Ganser, L.R., Ge, Y., Fare, C.M., Shorter, J., Leung, A.K.L., and Myong, S. (2022). Poly (ADP-ribose) drives condensation of FUS via a transient interaction. Mol. Cell *82*, 969–985.e11.

32. Teloni, F., and Altmeyer, M. (2016). Readers of poly (ADP-ribose): designed to be fit for purpose. Nucleic Acids Res. *44*, 993–1006.

33. Zhao, M., Kim, J.R., van Bruggen, R., and Park, J. (2018). RNA-binding proteins in amyotrophic lateral sclerosis. Mol. Cells *41*, 818–829.

34. Altmeyer, M., Neelsen, K.J., Teloni, F., Pozdnyakova, I., Pellegrino, S., Grøfte, M., Rask, M.-B.D., Streicher, W., Jungmichel, S., Nielsen, M.L., and Lukas, J. (2015). Liquid demixing of intrinsically disordered proteins is seeded by poly (ADP-ribose). Nat. Commun. *6*, 8088.

35. Patel, A., Lee, H.O., Jawerth, L., Maharana, S., Jahnel, M., Hein, M.Y., Stoynov, S., Mahamid, J., Saha, S., Franzmann, T.M., et al. (2015). A liquid-to-solid phase transition of the ALS protein FUS accelerated by disease mutation. Cell *162*, 1066–1077.

36. Schwartz, J.C., Wang, X., Podell, E.R., and Cech, T.R. (2013). RNA seeds higher-order assembly of FUS protein. Cell Rep. *5*, 918–925.

37. Singatulina, A.S., Hamon, L., Sukhanova, M.V., Desforges, B., Joshi, V., Bouhss, A., Lavrik, O.I., and Pastré, D. (2019). PARP-1 activation directs FUS to DNA damage sites to form PARG-reversible compartments enriched in damaged DNA. Cell Rep. *27*, 1809–1821.e5.

38. Sukhanova, M.V., Singatulina, A.S., Pastré, D., and Lavrik, O.I. (2020). Fused in sarcoma (FUS) in DNA Repair: Tango with poly (ADP-ribose) polymerase 1 and compartmentalisation of damaged DNA. Int. J. Mol. Sci. *21*, 7020.

39. Wang, H., and Hegde, M.L. (2019). New mechanisms of dna repair defects in fused in sarcoma–associated neurodegeneration: Stage set for dna repair-based therapeutics? J. Exp. Neurosci. *13*, 1179069519856358.

40. Rogelj, B., Easton, L.E., Bogu, G.K., Stanton, L.W., Rot, G., Curk, T., Zupan, B., Sugimoto, Y., Modic, M., Haberman, N., et al. (2012). Widespread binding of FUS along nascent RNA regulates alternative splicing in the brain. Sci. Rep. *2*, 603–610.

41. Kapeli, K., Pratt, G.A., Vu, A.Q., Hutt, K.R., Martinez, F.J., Sundararaman, B., Batra, R., Freese, P., Lambert, N.J., Huelga, S.C., et al. (2016). Distinct and shared functions of ALS-associated proteins TDP-43, FUS and TAF15 revealed by multisystem analyses. Nat. Commun. *7*, 12143.

42. Pankotai, T., and Soutoglou, E. (2013). Double strand breaks: hurdles for RNA polymerase II transcription? Transcription *4*, 34–38.

43. Dinant, C., Houtsmuller, A.B., and Vermeulen, W. (2008). Chromatin structure and DNA damage repair. Epigenet. Chromatin *1*, 9–13.

44. Van Attikum, H., and Gasser, S.M. (2009). Crosstalk between histone modifications during the DNA damage response. Trends Cell Biol. *19*, 207–217.

45. Liu, X., Niu, C., Ren, J., Zhang, J., Xie, X., Zhu, H., Feng, W., and Gong, W. (2013). The RRM domain of human fused in sarcoma protein reveals a non-canonical nucleic acid binding site. Biochim. Biophys. Acta *1832*, 375–385.

46. Loughlin, F.E., Lukavsky, P.J., Kazeeva, T., Reber, S., Hock, E.-M., Colombo, M., Von Schroetter, C., Pauli, P., Cléry, A., Mühlemann, O., et al. (2019). The solution structure of FUS bound to RNA reveals a bipartite mode of RNA recognition with both sequence and shape specificity. Mol. Cell *73*, 490–504.e6.

47. Ström, C.E., Johansson, F., Uhlén, M., Szigyarto, C.A.-K., Erixon, K., and Helleday, T. (2011). Poly (ADP-ribose) polymerase (PARP) is not involved in base excision repair but PARP inhibition traps a single-strand intermediate. Nucleic Acids Res. *39*, 3166–3175.

48. Lagerwerf, S., Vrouwe, M.G., Overmeer, R.M., Fousteri, M.I., and Mullenders, L.H.F. (2011). DNA damage response and transcription. DNA Repair *10*, 743–750.

49. Haines, N.M., Kim, Y.-I.T., Smith, A.J., and Savery, N.J. (2014). Stalled transcription complexes promote DNA repair at a distance. Proc. Natl. Acad. Sci. USA. *111*, 4037–4042.

50. Niaki, A.G., Sarkar, J., Cai, X., Rhine, K., Vidaurre, V., Guy, B., Hurst, M., Lee, J.C., Koh, H.R., Guo, L., et al. (2020). Loss of dynamic RNA interaction and aberrant phase separation induced by two distinct types of ALS/FTD-linked FUS mutations. Mol. Cell *77*, 82–94.e4.

51. Fu, H., Liu, R., Jia, Z., Li, R., Zhu, F., Zhu, W., Shao, Y., Jin, Y., Xue, Y., Huang, J., et al. (2022). Poly (ADP-ribosylation) of P-TEFb by PARP1 disrupts phase separation to inhibit global transcription after DNA damage. Nat. Cell Biol. *24*, 513–525.

52. Bonfiglio, J.J., Fontana, P., Zhang, Q., Colby, T., Gibbs-Seymour, I., Atanassov, I., Bartlett, E., Zaja, R., Ahel, I., and Matic, I. (2017). Serine ADP-ribosylation depends on HPF1. Mol. Cell *65*, 932–940.e6.

53. Gerstberger, S., Hafner, M., and Tuschl, T. (2014). A census of human RNA-binding proteins. Nat. Rev. Genet. *15*, 829–845.

54. Maucuer, A., Desforges, B., Joshi, V., Boca, M., Kretov, D.A., Hamon, L., Bouhss, A., Curmi, P.A., and Pastré, D. (2018). Microtubules as platforms for probing liquid–liquid phase separation in cells–application to RNA-binding proteins. J. Cell Sci. *131*, jcs214692.

55. Rengifo-Gonzalez, J.C., El Hage, K., Clément, M.J., Steiner, E., Joshi, V., Craveur, P., Durand, D., Pastré, D., and Bouhss, A. (2021). The cooperative binding of TDP-43 to GU-rich RNA repeats antagonizes TDP-43 aggregation. Elife *10*, e67605.

56. Kim, D.-S., Camacho, C.V., Nagari, A., Malladi, V.S., Challa, S., and Kraus, W.L. (2019). Activation of PARP-1 by snoRNAs controls ribosome biogenesis and cell growth via the RNA helicase DDX21. Mol. Cell *75*, 1270–1285.e14.

57. Alemasova, E.E., Moor, N.A., Naumenko, K.N., Kutuzov, M.M., Sukhanova, M.V., Pestryakov, P.E., and Lavrik, O.I. (2016). Y-box-binding protein 1 as a non-canonical factor of base excision repair. Biochim. Biophys. Acta *1864*, 1631–1640.

58. Martello, R., Mangerich, A., Sass, S., Dedon, P.C., and Bürkle, A. (2013). Quantification of cellular poly (ADP-ribosyl) ation by stable isotope dilution mass spectrometry reveals tissue-and drug-dependent stress response dynamics. ACS Chem. Biol. *8*, 1567–1575.

59. Alemasova, E.E., Naumenko, K.N., Kurgina, T.A., Anarbaev, R.O., and Lavrik, O.I. (2018). The multifunctional protein YB-1 potentiates PARP1 activity and decreases the efficiency of PARP1 inhibitors. Oncotarget *9*, 23349–23365.

60. Sun, S., Ling, S.-C., Qiu, J., Albuquerque, C.P., Zhou, Y., Tokunaga, S., Li, H., Qiu, H., Bui, A., Yeo, G.W., et al. (2015). ALS-causative mutations in FUS/TLS confer gain and loss of function by altered association with SMN and U1-snRNP. Nat. Commun. *6*, 6171.

61. Gilbertson, S., Federspiel, J.D., Hartenian, E., Cristea, I.M., and Glaunsinger, B. (2018). Changes in mRNA abundance drive shuttling of RNA binding proteins, linking cytoplasmic RNA degradation to transcription. Elife *7*, e37663.

62. Baumli, S., Endicott, J.A., and Johnson, L.N. (2010). Halogen bonds form the basis for selective P-TEFb inhibition by DRB. Chem. Biol. *17*, 931–936.

63. Chong, P.A., Vernon, R.M., and Forman-Kay, J.D. (2018). RGG/RG motif regions in RNA binding and phase separation. J. Mol. Biol. *430*, 4650–4665.

64. Ozdilek, B.A., Thompson, V.F., Ahmed, N.S., White, C.I., Batey, R.T., and Schwartz, J.C. (2017). Intrinsically disordered RGG/RG domains mediate degenerate specificity in RNA binding. Nucleic Acids Res. *45*, 7984–7996.

65. Dalvit, C., Fogliatto, G., Stewart, A., Veronesi, M., and Stockman, B. (2001). WaterLOGSY as a method for primary NMR screening: practical aspects and range of applicability. J. Biomol. NMR *21*, 349–359.

66. Mastrocola, A.S., Kim, S.H., Trinh, A.T., Rodenkirch, L.A., and Tibbetts, R.S. (2013). The RNA-binding protein fused in sarcoma (FUS) functions downstream of poly (ADP-ribose) polymerase (PARP) in response to DNA damage. J. Biol. Chem. *288*, 24731–24741.

67. Thandapani, P., O'Connor, T.R., Bailey, T.L., and Richard, S. (2013). Defining the RGG/RG motif. Mol. Cell *50*, 613–623.

68. Takata, H., Hanafusa, T., Mori, T., Shimura, M., Iida, Y., Ishikawa, K., Yoshikawa, K., Yoshikawa, Y., and Maeshima, K. (2013). Chromatin compaction protects genomic DNA from radiation damage. PLoS One *8*, e75622.

69. Amouroux, R., Campalans, A., Epe, B., and Radicella, J.P. (2010). Oxidative stress triggers the preferential assembly of base excision repair complexes on open chromatin regions. Nucleic Acids Res. *38*, 2878–2890.

70. Krüger, A., Bürkle, A., Hauser, K., and Mangerich, A. (2020). Real-time monitoring of PARP1-dependent PARylation by ATR-FTIR spectroscopy. Nat. Commun. *11*, 2174.

71. Naumenko, K.N., Sukhanova, M.V., Hamon, L., Kurgina, T.A., Alemasova, E.E., Kutuzov, M.M., Pastré, D., and Lavrik, O.I. (2020). Regulation of poly (ADP-Ribose) polymerase 1 activity by Y-Box-Binding protein 1. Biomolecules *10*, 1325.

72. Larsen, S.C., Hendriks, I.A., Lyon, D., Jensen, L.J., and Nielsen, M.L. (2018). Systems-wide analysis of serine ADP-ribosylation reveals widespread occurrence and site-specific overlap with phosphorylation. Cell Rep. *24*, 2493–2505.e4.

73. Slade, D. (2020). PARP and PARG inhibitors in cancer treatment. Genes Dev. *34*, 360–394.

74. Harrison, A.F., and Shorter, J. (2017). RNA-binding proteins with prion-like domains in health and disease. Biochem. J. *474*, 1417–1438.

75. Qamar, S., Wang, G., Randle, S.J., Ruggeri, F.S., Varela, J.A., Lin, J.Q., Phillips, E.C., Miyashita, A., Williams, D., Ströhl, F., et al. (2018). FUS phase separation is modulated by a molecular chaperone and methylation of arginine cation-π interactions. Cell *173*, 720–734.e15.

76. Hofweber, M., Hutten, S., Bourgeois, B., Spreitzer, E., Niedner-Boblenz, A., Schifferer, M., Ruepp, M.-D., Simons, M., Niessing, D., Madl, T., and Dormann, D. (2018). Phase separation of FUS is suppressed by its nuclear import receptor and arginine methylation. Cell *173*, 706–719.e13.

77. Deng, H., Gao, K., and Jankovic, J. (2014). The role of FUS gene variants in neurodegenerative diseases. Nat. Rev. Neurol. *10*, 337–348.

78. Groth, A., Rocha, W., Verreault, A., and Almouzni, G. (2007). Chromatin challenges during DNA replication and repair. Cell *128*, 721–733.

79. Amé, J.C., Héberlé, É., Camuzeaux, B., Dantzer, F., and Schreiber, V. (2017). Purification of recombinant human PARG and activity assays. Methods Mol. Biol. *1608*, 395–413.

80. Panzeter, P.L., and Althaus, F.R. (1990). High resolution size analysis of ADP-ribose polymers using modified DNA sequencing gels. Nucleic Acids Res. *18*, 2194.

STAR★METHODS

KEY RESOURCES TABLE

REAGENT or RESOURCE	SOURCE	IDENTIFIER
Antibodies		
Rabbit polyclonal anti-PARP1	Abcam	Cat#ab227244
Rabbit polyclonal anti-gamma H2A.X (phosphor S139)	Abcam	Cat#ab11174
Rabbit polyclonal anti-FUS	Novus Biologicals	Cat#NB100-565
Mouse monoclonal anti-Histone H3	Santa Cruz Biotechnology	Cat#sc-517576
Mouse monoclonal anti-HA-Tag (F-7)	Santa Cruz Biotechnology	Cat#sc-7392
Rabbit polyclonal anti-TDP43 (C-terminal)	Proteintech	Cat#12892-1-AP
Mouse monoclonal anti-PCNA (PC10)	Novus Biologicals	Cat#NB500-106SS
Rat monoclonal anti-BrdU [BU1/75 (ICR1)]	Abcam	Cat#ab6326
Mouse monoclonal anti-TARDBP	Abnova	Cat#H00023435-M01
Mouse monoclonal anti-HuR (3A2)	Invitrogen	Cat#39-0600
Rabbit monoclonal anti-HUR (D9W7E)	Cell Signaling Technology	Cat#12582
Mouse monoclonal anti-FUS (CL0190)	Novus Biologicals	Cat#NBP2-52874
Rabbit monoclonal anti-Poly/Mono-ADP Ribose (E6F6A)	Cell Signaling Technology	Cat#83732
Rabbit polyclonal anti-PAR	R&D Systems	Cat#4336-BPC-100
Mouse monoclonal anti-β-tubulin antibody	Produced from E7 hybridoma clone from ATCC.	N/A
IRDye® 800CW Goat anti-Rabbit IgG Secondary Antibody	LI-COR	Cat#926-32211
IRDye® 680RD Goat anti-Mouse IgG Secondary Antibody	LI-COR	Cat#926-68070
Goat anti-Rabbit IgG (H + L) Cross-Adsorbed Secondary Antibody, Alexa Fluor™ 594	Invitrogen	Cat#A-11012
Goat anti-Mouse IgG (H + L) Cross-Adsorbed Secondary Antibody, Alexa Fluor™ 594	Invitrogen	Cat#A-11005
Goat anti-Rat IgG (H + L) Cross-Adsorbed Secondary Antibody, Cyanine3	Invitrogen	Cat#A10522
Donkey anti-Rabbit IgG (H + L) Cross-Adsorbed Secondary Antibody, DyLight™ 488	Invitrogen	Cat#SA5-10038
Donkey anti-Mouse IgG (H + L) Highly Cross-Adsorbed Secondary Antibody, Alexa Fluor™ 594	Invitrogen	Cat#A-21203
Bacterial and virus strains		
Escherichia coli BL21(DE3)	Invitrogen	Cat#C600003
Rosetta™(DE3)pLysS Competent Cells	Novagen	Cat#70956
TOP10 Chemically Competent E. coli	Invitrogen	Cat#C404010
Chemicals, peptides, and recombinant proteins		
Restriction Enzyme AscI	Thermo Fisher Scientific	Cat#FD1894
Restriction Enzyme DpnI	Thermo Fisher Scientific	Cat#
Restriction Enzyme EcoRV	Thermo Fisher Scientific	Cat#FD0303
Restriction Enzyme PacI	Thermo Fisher Scientific	Cat#FD2204
Restriction Enzyme NdeI	Thermo Fisher Scientific	Cat#FD0583
Restriction Enzyme XhoI	Thermo Fisher Scientific	Cat#FD0694
Phusion™ High-Fidelity DNA Polymerase	Thermo Fisher Scientific	Cat# F530S

(*Continued on next page*)

Continued

REAGENT or RESOURCE	SOURCE	IDENTIFIER
Lipofectamine 2000	Thermo Fisher Scientific	Cat#11668019
Paraformaldehyde, 16% w/v aq. soln., methanol free	Thermo Fisher Scientific	Cat#043368
Actinomycin D (ActD)	Thermo Fisher Scientific	Cat#11805017
Olaparib (AZD2281, Ku-0059436)	Apexbio Technology	Cat#A4154
5-Bromouridine	Sigma-Aldrich	Cat#850187
5,6-Dichlorobenzimidazole 1-β-D-ribofuranoside (DRB)	Sigma-Aldrich	Cat#D1916
Oxaliplatin	Sigma-Aldrich	Cat#O9512
DAPI/Antifade Solution	Sigma-Aldrich	Cat#S7113
DNase I, RNase-free	Thermo Fisher Scientific	Cat#EN0521
Ribonuclease Inhibitor	Euromedex	Cat#09-0312
PARG inhibitor (PDD00017273)	Sigma-Aldrich	Cat#SML1781
cOmplete ULTRA Tablets, Mini, EASYpack Protease Inhibitor Cocktail	Roche	Cat#5892970001
PMSF	Sigma-Aldrich	Cat#93482
BSA	Sigma-Aldrich	Cat#A2153
β-Nicotinamide mononucleotide	Sigma-Aldrich	Cat#N3501
NAD+, Free Acid	Sigma-Aldrich	Cat#481911
Solution ATP	Thermo Fisher Scientific	Cat#R0441
α[^{32}P]ATP (3000 Ci/mmol)	Laboratory of Biotechnology (ICBFM SB RAS, Novosibirsk, Russia)	N/A
Nicotinamide mononucleotide adenylyl transferase (NMNAT)	Dr. S. I. Shram (Institute of Molecular Genetic RAS, Moscow)	N/A
HisTrap Fast Flow	GE Healthcare	Cat#GE17-5255-01
HiTrap Heparin High Performance	GE Healthcare	Cat#GE17-0407-01
Ni-NTA Agarose	Quiagen	Cat#30210
PD-10 desalting columns	GE Healthcare	Cat#17085101
Critical commercial assays		
Gateway™ LR Clonase™ II Enzyme mix	Invitrogen	Cat#11791
QuikChange II Site-Directed Mutagenesis Kit	Agilent	Cat#200523
Duolink® *In Situ* PLA® Probe Anti-Rabbit PLUS	Sigma-Aldrich	Cat#DUO92002
Duolink® *In Situ* PLA® Probe Anti-Mouse MINUS	Sigma-Aldrich	Cat#DUO92004
Duolink® *In Situ* Detection Reagents Red	Sigma-Aldrich	Cat#DUO92008
Experimental models: Cell lines		
Human: HeLa	ATCC	Cat#CRM-CCL-2
Human: HEK-293	ATCC	Cat#CRL-1573
Oligonucleotides		
Primers for PCR	This paper	Table S1
AllStar Negative Control siRNA	QIAGEN	Cat#1027281
siRNA targeting sequence: FUS: 5'-(AAUAACGAGGGUAACACUGGG)dTdT-3′	Eurofins Genomics	N/A
siRNA targeting sequence: TDP-43: 5'-(GCUCUAAUUCUGGUGGAGCAA)dTdT-3′	Eurofins Genomics	N/A
siRNA targeting sequence: HuR	QIAGEN	Cat#SI00300139
DNA oligonucleotide: A20d	Eurofins Genomics	N/A
DNA oligonucleotide: T10	Eurofins Genomics	N/A
RNA oligonucleotide: A20r	Eurogentec	N/A

(*Continued on next page*)

Continued

REAGENT or RESOURCE	SOURCE	IDENTIFIER
RNA oligonucleotide: hnRNP RNA loop: GGCAGAUUACAAUUCUAUUUGCC	Eurogentec	N/A
Calf thymus DNA	Sigma-Aldrich	Cat#D4522
Recombinant DNA		
pEGFP(C1)-PP1alpha	Addgene	Cat#44224
pCDNA3-HA-PSPC1	Addgene	Cat#101764
pcDNA3.1-HA-NONO	Addgene	Cat#127655
pGEX4T-hLIG3	Addgene	Cat#81055
pQE30-hPolB	Addgene	Cat#70761
pET16b -XRCC1	Dr. Pablo J. Radicella (Institute of Molecular and Cellular Radiobiology, Fontenay aux Roses, France)	N/A
pET15b-hLigI	N/A	N/A
pET32a-PARP1	Dr. M. Satoh (Laval University, Canada)	N/A
pXC53-hAPE1	Dr. S.H. Wilson (NIEHS, NIH, USA)	N/A
PEF-DEST51-PARP1-RFP-MBD	This paper	N/A
PEF-DEST51-LIG3-RFP-MBD	This paper	N/A
PEF-DEST51-XRCC1-RFP-MBD	This paper	N/A
PEF-DEST51-POLB-RFP-MBD	This paper	N/A
PEF-DEST51-NONO-RFP-MBD	This paper	N/A
PEF-DEST51-PP1α--RFP-MBD	This paper	N/A
PEF-DEST51-LIG1-RFP-MBD	This paper	N/A
PEF-DEST51-APE1-RFP-MBD	This paper	N/A
PEF-DEST51-TOP1-RFP-MBD	This paper	N/A
PEF-DEST51-FUS-RFP-MBD	(Maucuer et al.)	N/A
PEF-DEST51-EWSR1-RFP-MBD	This paper	N/A
PEF-DEST51-TAF15-RFP-MBD	This paper	N/A
PEF-DEST51-G3BP1-RFP-MBD	This paper	N/A
PEF-DEST51-LIN28-RFP-MBD	(Maucuer et al.)[54]	N/A
PEF-DEST51-SAM68-RFP-MBD	(Maucuer et al.)[54]	N/A
PEF-DEST51-HuR-RFP-MBD	(Maucuer et al.)[54]	N/A
PEF-DEST51-TDP-43-RFP-MBD	(Maucuer et al.)[54]	N/A
PEF-DEST51-PARP1-GFP-MBD	This paper	N/A
PEF-DEST51-PARP1(K893I)-GFP-MBD	This paper	N/A
PEF-DEST51-FUS-GFP-MBD	This paper	N/A
pcDNA3.1-FUS-HA	This paper	N/A
pcDNA3.1-FUSΔRRMTDP43-HA	This paper	N/A
pcDNA3.1-FUS(K315A/K316A)-HA	This paper	N/A
pcDNA3.1-FUS(N284A)-HA	This paper	N/A
pcDNA3.1-FUS(D342A)-HA	This paper	N/A
pcDNA3.1-FUS(D343A)-HA	This paper	N/A
pcDNA3.1-TDP-43-HA	This paper	N/A
pcDNA3.1-HuR-HA	This paper	N/A
pET-28-a-FUS_275-385	This paper	N/A
pET-28-a-TDP-RRM2_176-277	(Rengifo-Gonzalez et al.)[55]	N/A

(*Continued on next page*)

Continued

REAGENT or RESOURCE	SOURCE	IDENTIFIER
pET-22-b-FUS-FL	(Singatulina et al.)[37]	N/A
pET-22-b-FUS-FL-D343A	This paper	N/A
Software and algorithms		
ImageJ 1.50i (Java 1.8.0_131 (32-bit))	Wayne Rasband, NIH, USA	https://imagej.nih.gov/ij/
Quantity One 1-D Analysis Software	Bio-Rad Laboratories	https://www.bio-rad.com/fr-fr/product/quantity-one-1-*d*-analysis-software?ID=1de9eb3a-1eb5-4edb-82d2-68b91bf360fb
MATLAB R2022a	The MathWorks, Inc.	https://fr.mathworks.com/products/matlab.html
Harmony High-Content Imaging and Analysis Software	Perkin Elmer Inc.	https://www.perkinelmer.com/product/harmony-4-8-office-hh17000001

RESOURCE AVAILABILITY

Lead contact

Further information and requests for resources reagents should be directed to and will be fulfilled by the Lead Contact, David Pastré (david.pastre@univ-evry.fr).

Materials availability

Plasmids generated in this study are available from the lead contact with a completed Materials Transfer Agreement.

Data and code availability

- All data reported in this paper will be shared by the lead contact upon request.
- This paper does not report original code.
- Any additional information required to reanalyze the data reported in this paper is available from the lead contact upon request.

EXPERIMENTAL MODEL AND STUDY PARTICIPANT DETAILS

Cell culture

Human Embryonic Kidney 293, (HEK293) and HeLa cell lines (American Type Collection, USA) were cultured at 37°C in a humidified atmosphere with 5% CO2 and maintained in high glucose formulation of DMEM (Life Technologies) supplemented with penicillin G 100U/mL, streptomycin 100 μg/mL and fetal bovine serum (FBS) 10% (Thermofisher). The cells were cultured in 96-well plates (PhenoPlate-96, PerkinElmer) at a density of 1.3×10^4 for immunofluorescence or in 10-cm Petri dishes for the cell extract preparation.

METHOD DETAILS

Preparation of plasmids for expression in mammalian and E.coli cells

Plasmids harboring cDNA of the full length FUS, TDP43, HuR, G3BP1, Lin28a, SAM68 genes fused with RFP-MBD (Microtubule-Binding Domain of Tau) and/or GFP-MBD were obtained previously.[54] The constructs with C-terminal RFP-MBD fusion harboring cDNA of the full length PARP1, Lig3, XRCC1, POLβ, NONO, PP1α, Lig1, APE1, TOP1, EWSR1 or TAF15 genes were engineered using the gateway strategy as previously described.[54] In brief, cDNAs encoding the proteins were amplified using primers containing PacI and AscI restriction sites and inserted into the backbone entry plasmid RFP-MBD-pCR8/GW/TOPO previously digested with the corresponding restriction enzymes. Sequences encoding gene of interest fused with RFP-MBD were cloned from pCR8/GW/TOPO plasmids into the Gateway pEF-Dest51 plasmid (Invitrogen) using LR recombination reactions (Invitrogen) according to the manufacturer's protocol.

Mutations K893I within the PARP-1 coding sequence was carried out by site-directed mutagenesis directly on the PARP1-RFP-MBD-PEF-DEST51 expression plasmid using the "Quikchange II XL site-directed mutagenesis kit" (Stratagene) and appropriate oligonucleotides (Eurofins Genomics). The sequence of mutant PARP1 gene was confirmed by DNA sequencing (Eurofins Genomics).

To produce the plasmids encoding the full length FUS, TDP43 or HuR fused to HA-tag, the corresponding cDNAs were amplified by PCR using primers containing NdeI and XhoI restriction sites and inserted into HA-pcDNA3.1 vector (Table S1). For the preparation of K315A/K316A, N284A, D342A and D343A FUS mutants site-directed mutagenesis of FUS coding gene was performed directly on the

HA-FUS-pcDNA3.1 expression vector by using the ''Quikchange II XL site-directed mutagenesis kit'' (Stratagene) and appropriate oligonucleotides (Eurofins Genomics). The introduced mutations were verified by DNA sequencing (Eurofins Genomics).

For the preparation of HA-FUSΔRRMTDP43-pcDNA3.1 plasmid, first, the cDNAs encoding amino acids 1–275 and 385–526 were amplified by PCR using primers containing NdeI, EcoRV and EcoRV, XhoI restriction sites respectively and inserted into HA-pcDNA3.1 vector previously digested with the NdeI and XhoI restriction enzymes. Then the cDNA encoding RRM1 domain of TDP43 was amplified by PCR using primers containing EcoRV restriction sites and inserted into HA-FUS-pcDNA3.1 plasmid with insertions encoding amino acids 1–275 and 385–526. The inserted cDNAs and reading frames for all prepared plasmids were verified by DNA sequencing (Eurofins Genomics).

Site-directed mutagenesis of the FUS RRM was carried out directly on the pET-28-a-FUS_275–385 or pET-22-b-FUS-FL expression plasmid by using the 'Quikchange II XL site-directed mutagenesis kit' (Stratagene) and appropriate oligonucleotides (Eurofins Genomics). The introduced mutations (N284A, K315A/K316A, D342A, and D343A) were checked by DNA sequencing (Eurofins Genomics).

Plasmid transfection, siRNA treatment and addback experiments

HeLa cells were grown in 96-well plates and were transiently transfected with 0.2 μg of recombinant plasmid for each well using lipofectamine 2000 (Thermofisher) transfection reagent for 24–48 h according to the manufacturer's instructions. For the silencing of FUS, TDP-43 or HuR, HeLa cells were transfected with 0.15 μg of corresponding small interfering RNA (siRNA) duplex using Lipofectamine 2000 for 24 h. A non-targeting sequence siRNA (AllStars Negative Control siRNA) was used as a negative control. For the addback experiments, firstly, HeLa cells were transfected with siRNA targeting endogenous FUS for 24 h and, secondly, the cells were transfected with the plasmid encoding wild type or mutant FUS, as indicated. The efficiency of transfection with HA-FUS overexpressing plasmid was measured at the single-cell level using antibodies to FUS and HA-tag and was calculated as the increase of total FUS expression for the HA-FUS overexpressing cells compared to the cells with endogenous FUS expression level (Figure S4C). The efficiency of transfection with siRNA was calculated as the difference in FUS expression for the cells treated with a non-targeting sequence siRNA and siRNA targeting FUS (Figure S4D).

For oxidative stress induction, HeLa cells were treated with 10, 30, 100 or 300 μM hydrogen peroxide (H_2O_2) and incubated at 37°C for 30 min. When indicated, cells were pre-treated with 5 μg/mL actinomycin D (ActD) at 37°C for 30 min before H_2O_2 treatment.

Microtubule bench assay

HeLa cells were grown in 96-well plates and were co-transfected with 0.4 μg GFP expression plasmid or 0.2 μg RFP expression plasmid using lipofectamine 2000 (Thermofisher) transfection reagent for 24 h according to the manufacturer's instructions. After 24 h of transfection cells were fixed first with ice-cold methanol for 10 min at −20°C, then with 4% paraformaldehyde (PFA) in PBS for 10 min at 37 °C. The cells were washed 3 times with PBS and stained with 300 nM DAPI to visualize the nuclei. The cell images were obtained with the Opera Phenix Plus High Content Screening System (PerkinElmer) on 40x magnification with a liquid-immersed lens.

High-content imaging assay and analysis

Cells were washed with PBS, fixed first with ice-cold methanol for 10 min at −20°C, then with 4% paraformaldehyde (PFA) in PBS for 10 min at 37 °C. After washing with PBS, cells were kept with blocking buffer (50 mM Tris pH 7.5, 100 mM NaCl, 2% BSA, 0.15% Triton X-100) for 30 min at 37 °C to permeabilize the cells and reduce nonspecific recognition by antibodies. Blocking buffer was removed and cells were washed and then incubated with corresponding primary antibodies overnight at 4 °C. After that, the cells were washed 3 times with PBS and incubated for 1 h with fluorochrome (Alexa Fluor488 and −594)-coupled secondary antibodies in blocking buffer. After final washing with PBS, the cells were stained with 300 nM DAPI to visualize the nuclei. The cell images were obtained with the Opera Phenix Plus High Content Screening System (PerkinElmer) on 20x or 40x magnification in the confocal mode. Image capture was performed using three channels.

a. DAPI (excitation 405 nm; emission 435–480 nm);
b. Cy3 (excitation 561 nm; emission 570–630 nm);
c. EGFP (excitation 488 nm; emission 500–550 nm).

Images were analyzed using the PerkinElmer Harmony v4.8 software. DAPI signal was used for nuclei detection. The signal fluorescence intensity of silenced/overexpressed proteins or PAR was measured in the nucleus. The relative increase in nuclear PAR level in protein overexpressing cells was calculated as the ratio of the nuclear PAR level in cells overexpressing HA-tagged protein (HA-signal >6.8 and <9 in log scale) to the nuclear PAR level in cells with low level of protein expression (HA-signal <6.5 in log scale). The corresponding scatterplots and violin plots were created using MATLAB R2022a software (Figures 1D, 2A–C, 5B, C, and Figures S3–S8).

In situ RNA hybridization

To visualize poly(A) mRNA using *in situ* hybridization, after fixation HeLa cells were incubated with Cy3-labelled poly(dT) in hybridization buffer (2×SSC buffer, 1 mg/mL yeast tRNA, 0.005% BSA, 10% dextran sulfate, 25% formamide) for 2 h at 37°C. Wash steps were performed using 4× and then 2× SSC buffer (0.88% sodium citrate, 1.75% NaCl, pH 7.0).

5-Bromouridin (BrU) incorporation analysis

After 24 h of transfection with FUS-HA expressing plasmid HeLa, cells were incubated with 5mM BrU for 35 min at 37°C and H_2O_2 (30, 100 or 300 μM) for 30 min. Cells were fixed with ice-cold methanol for 10 min at −20°C, washed with PBS and fixed with 4% paraformaldehyde (PFA) for 10 min at 37°C. After cells were washed 3 times with PBS and kept with blocking buffer (50 mM Tris pH 7.5, 100 mM NaCl, BSA 2%, 0.15% Triton X-100) for 30 min at 37°C. The primary anti-BrdU monoclonal rat antibodies (ab6326, Abcam) recognising both BrdU and BrU were diluted 1:1000 in blocking buffer and applied to cells for incubation overnight at 4 °C. After PBS washings, the secondary goat anti-rat antibody (Alexa 594, Invitrogen) were diluted 1:1000 in blocking buffer and added to cells for 1 h at room temperature. After final washes with PBS, the cells were stained with 300 nM DAPI to visualize the nuclei. The anti-BrdU fluorescence was detected and measured automatically using Opera Phenix Plus High Content Screening System (PerkinElmer) and the Harmony v4.8 software (Figure S7B).

Proximity ligation assay (PLA)

Proximity ligation assay was performed using Duolink PLA technology Kit (Sigma) according to the manufacturer's recommendations. HeLa cells were grown in a 96-well plate at a density of 1.3×10^4 cells per well and transfected with corresponding plasmids for 24 h. The cells were washed with PBS for 5 min, then fixed with 4% PFA for 30 min at 37°C and washed with PBS. The cells were permeabilized using 0.2% Triton X-100 in PBS for 10 min and incubated with blocking solution for 60 min at 37°C. The samples were incubated with anti-HA and anti-PARP1 primary antibodies in the supplied buffer at 4°C overnight, then washed 3 times with 0.2% Triton X-100 in PBS. The PLUS and MINUS PLA probes were diluted 1:5 in corresponding buffers, provided by manufacturer, and incubated with cells for 60 min at 37°C, then the samples were washed 3 times with PBS. The DNA ligase was diluted 1:40 in the ligation buffer (diluted 1:5) and added to the samples followed by incubation for 30 min at 37°C, then the samples were washed 2 times with PBS. The samples were incubated in the amplification solution (1:80 DNA polymerase in the amplification solution diluted 1:5) for 100 min at 37°C and washed 2 times with PBS for 10 min. The samples were stained with DAPI. The cell images were obtained with the Opera Phenix Plus High Content Screening System (PerkinElmer) and analyzed with Harmony v4.8 software.

Isolation of chromatin-bound proteins and Western blot analysis

HEK293 cells were grown on 10 cm Petri dishes, transfected and treated with plasmids and reagents as indicated in the Figure Legends. The preparation of chromatin bound fraction and soluble fraction was performed as described previously.[78] Briefly, soluble proteins of HEK293 cells were isolated by extracted with Triton X-100, namely, the cells were incubated with 3 volumes of 0.5% Triton X-100 in CSK buffer (10 mM PIPES pH 7, 100 mM NaCl, 300 mM sucrose, 3 mM $MgCl_2$, 1mM DTT, protease inhibitors) for 20 min on ice, and then were centrifuged for 5 min at 1500 g, the supernatant was collected and used for WB as a free fraction. The pellet was washed with 0.1% Triton X-100 in CSK buffer, resuspended in DNase I digest buffer (10 mM Tris-HCl pH 7.8, 10 mM NaCl, 5 mM $MgCl_2$, protease inhibitors), incubated with DNase I (35U in 50 μL of DNase I digest buffer) for 20 min at 37°C and centrifuged for 10 min at 16000 g; the supernatant was used for WB as a chromatin bound fraction.

For Western blot analysis, first, proteins were separated on 10% SDS-PAGE and transferred onto a PVDF membrane. After that, the membrane was stained with 0.2% Ponceau-S red to detect proteins. The stained membrane was washed with 1% CH3COOH for fixation, then washed with TBS-Tween buffer (20 mM Trizma Base, 143 mM NaCl, pH 7.6, 1% Tween 20) and blocked with 5% non-fat dry milk for 1 h at room temperature. Then, the membrane was washed again with TBS-Tween buffer and incubated overnight at 4 °C with indicated primary antibodies. After a wash step, the secondary antibody (LI-COR IRDye, IRDye 800CW goat-*anti*-rabbit 1:5000, IRDye 680RD goat-*anti*-mouse 1:5000) was added to the membrane in TBS-Tween buffer for 45 min at room temperature. The membrane was washed with TBS-Tween buffer, bound antibodies were detected with Amersham Typhoon Bioimager.

Recombinant protein production and purification

Recombinant PARP1 was overexpressed in *E. coli* Rosetta (DE3) pLysS (Novogen, catalog # 70956-3) and purified by Ni-NTA agarose (GE Healthcare United States, catalog # GE17-5255-01) affinity chromatography, HiTrap Heparin High Performance (GE Healthcare, United States, catalog # GE17-0407-01) affinity chromatography, and deoxyribonucleic acid−cellulose (single-stranded calf thymus DNA) (Sigma-Aldrich, United States, catalog #D8273) affinity chromatography as described previously.[71] The recombinant His_6-tagged FUS-RRM fragment (aa 275–385) from the human full-length FUS was first cloned into the pET-28-a expression vector while the recombinant His_6-tagged TDP-RRM2 (aa 176–277) fragment was cloned as previously described.[55] BL21 (DE3) competent E. coli cells were transformed with the constructed plasmid pET-28-a-FUS_275–385 or pTDP-RRM2_176–277 and grown at 37°C in minimal medium M9 supplemented with $^{15}NH_4Cl$ and 50 μg/mL of kanamycin. The protein expression was induced by the addition of IPTG to a final concentration of 1 mM at OD_{600} = 0.7. The culture was grown at 37°C for 4 h and cells were harvested and washed with 20 mL of cold buffer consisting of 30 mM Tris-HCl, pH 7.6, and 100mM KCl. The cell pellet was resuspended in 20 mL of buffer A (20 mM Tris-HCl, pH 7.6, 1.5 M KCl, 1 mM TCEP, 1 mM PMSF, and EDTA-free protease inhibitor Cocktail (Roche)) and cells were disrupted by sonication on ice (Bioblock Vibracell sonicator, model 72412). The cell lysate was centrifuged at 4°C for 30 min at 150,000×g in a TL100 Beckman centrifuge. The supernatant was used for purification experiments.

The FUS RRM (WT and N284A, K315A/K316A, D342A, D343A mutants) and TDP-43 RRM fragments were purified following the manufacturer's recommendations (Qiagen). Briefly, the supernatant was incubated with Ni^{2+} - NTA-agarose (Qiagen) (20 mg of proteins/mL of resin) pre-equilibrated in buffer A for 2 h at 4°C. The resin was then washed extensively with buffer A, containing 10 mM

and 20 mM imidazole. The protein was eluted with an imidazole linear gradient (50–500 mM) in buffer A. Pure protein fractions were pooled and buffer exchanged against NMR buffer (15 mM K_2HPO_4/KH_2PO_4, pH 6.8, 25 mM KCl and 1 mM TCEP) by using a PD-10 column (GE Healthcare). The final preparations were snap-frozen and stored at - 80°C.

Recombinant full-length FUS WT or FUS D343A mutant were overexpressed in *E. coli* BL21(DE3) and purified as previously described.[37]

The purity of the proteins was monitored at all stages of the purification by SDS-PAGE (Laemmli, 1970).

Radioactive assay of protein PARylation *in vitro*

[^{32}P]-NAD$^+$ labeled on the adenylate phosphate was synthesized in a reaction mixture (100μL) containing 2 mM β-Nicotinamide mononucleotide, 1 mM ATP and 0.25 mCi of [α-32P]-ATP (1000 Ci/mmol), 1.5 mg/mL nicotinamide mononucleotide adenylyl transferase (NMNAT), 25 mM Tris- HCl (pH 7.5), and 20 mM $MgCl_2$ was incubated for 1 h at 37°C. The enzyme was denatured by heating at 65°C for 10 min and precipitated proteins were removed by centrifugation.

An *in vitro* poly(ADP-ribosyl)ation of full-length FUS WT, FUS D343A mutant assay was performed in the reaction mixtures (12 μL) containing 20 mM Tris-HCl, pH 7.5, 25 mM NaCl, 1 mM DTT, 400 mM Urea, 0.1 OD_{260}/mL of DNase I-activated calf thymus DNA, 100 nM PARP-1, 0.3 mM NAD$^+$, 0.4 μCi [^{32}P]-NAD$^+$ and 50, 200, 800 or 3000 nM of FUS WT or FUS(D343A). The reactions were initiated by the addition of NAD$^+$. The reaction mixtures were incubated at 37°C for 1, 3, 7, 15 or 30 min and stopped by adding SDS-sample buffer and heating for 5 min at 90°C.

An *in vitro* poly(ADP-ribosyl)ation of RRM fragments was performed in the reaction mixture (15 μL) containing 20 mM Tris-HCl, pH 7.5, 25 mM NaCl, 1 mM DTT, 0.1 OD_{260}/mL of DNase I-activated calf thymus DNA, 100 nM PARP-1, 0.3 mM NAD+, 0.4 μCi [^{32}P]-NAD$^+$ and 4, 8, or 16 μM of RRM fragment as indicated. The reactions were initiated by the addition of NAD$^+$. The reaction mixtures were incubated at 37°C for 30 min and stopped by adding SDS-sample buffer and heating for 5 min at 90°C.

The reaction mixtures were analyzed by 10% SDS-PAGE and the PARylated proteins were visualised by phosphorimaging by means of Typhoon FLA 7000 (GE Healthcare, Chicago, IL, USA) and/or colloidal Coomassie staining.

PAR used for NMR analysis was synthesized in the reaction mixture (3 mL) consisting of 50 mM Tris- HCl (pH 7.5), 2 mM DTT, 4 mM $MgCl_2$, 1 μM DNA duplex (30 bp), 0.35 μM PARP1 and 0.5 mM NAD$^+$ + 0.05 μCi [^{32}P]-NAD$^+$ (was added for the visualisation). The mixture was incubated at 37°C for 1 h. After that, the purification of PAR was processed as described previously.[79] The bulk PAR was analyzed by gel electrophoresis using modified DNA sequencing gels as described.[80] PAR concentration was estimated by measurement of absorbance at 258 nm (A258) and application of an extinction coefficient of 13.5 $mM^{-1}cm^{-1}$ for ADP-ribose (ADPr).

NMR analysis

All NMR Experiments were performed on 60 μL samples prepared in 25 mM K_2HPO_4/KH_2PO_4 buffer pH 6.8, using 1.7 mm diameter capillary tubes. NMR spectra were acquired at 298K on a Bruker AVIII HD 600MHz spectrometer equipped with a triple-resonance cryoprobe.

Interactions of the purified ^{15}N protein fragments (FUS RRM, TDP-43 RRM2 and HuR RRM1) with protein-free PAR (Figure S9C) purified as described previously,[37] DNA (*Eurofins*) or RNA (*Eurogentec*) oligonucleotides (A20r, A20d, T10 and hnRNPA2/B1 RNA stem loop) were investigated using 2D ^{1}H-^{15}N SOFAST-HMQC experiments. The spectra were recorded on 50 μM protein samples alone and in presence of 90 μM PAR or oligonucleotides. Data were acquired with 16 dummy scans, 256 scans, 2048 points along the direct dimension, 128 t1 increments and a relaxation delay of 0.2 s. Shaped pulse length and power were calculated by considering an amide 1H bandwidth of 4.5 ppm and a chemical shift offset of 8.25 ppm. The same experimental conditions were used for studying the interaction of the FUS RRM mutants (N284A, K315/216A, D342A and D343A) with PAR. From the 2D ^{1}H-^{15}N SOFAST-HMQC spectra, chemical shift perturbations (CSPs) were calculated as $\Delta\delta = \sqrt{0.5(0.14\cdot\Delta\delta^{15}N)^2+(\Delta\delta^{1}H)^2}$. The overall binding efficiency between the protein fragments and the different ligands was evaluated by calculating the standard deviation (σ) of the CSPs.

In order to analyze the binding specificity of FUS RRM:PAR interaction, NMR competition assays were performed using 2D ^{1}H-^{15}N SOFAST-HMQC experiments recorded on equimolar samples (50 μM) of ^{15}N FUS RRM or TDP-43 RRM2 in presence of PAR, T10 or a mixture of both ligands. These same samples have been used to record WaterLOGSY experiments (1024 scans). Control experiments were carried out without and with the PAR alone. The binding specificity was evaluated by the modification of ligand peak intensities (more positive or less negative) upon protein binding. A last NMR competition assay has been performed by recording 2D ^{1}H-^{15}N SOFAST-HMQC experiment on a sample containing preformed TDP-43 RRM:PAR complex on which FUS RRM has been added.

NMR experiments have been also designed to analyze the effect of FUS RRM and its D343 mutant on PARylation catalyzed with PARP-1. 1D (64 scans) and 2D ^{1}H-^{15}N SOFAST-HMQC (32 scans) spectra has been recorded at different times (0, 10′, 50′, 1h 30′ and 3h) on a reaction mixtures containing 50 μM ^{15}N FUS RRM or D343, 1 μM PARP-1, 3 mM NAD$^+$, 25 mM $MgCl_2$ in HEPES buffer (20 mM, pH 7.5). The PARP-1 activation was initiated by the addition of DNA duplex (30 bp) to a final concentration of 1 μM and it could be easily followed on the 1D spectra by the observation of NAD$^+$ consumption and nicotinamide appearance over time.

QUANTIFICATION AND STATISTICAL ANALYSIS

Analysis of cell by HCS fluorescence microscopy

Images were analyzed using the PerkinElmer Harmony v4.8 software.

To measure sub-compartmentalization in the system with both proteins fused to GFP/RFP-MBD, the cell image analysis was carried out using the PerkinElmer Harmony v4.8 software. First, nuclei, cytoplasm and spots of proteins fused to GFP/RFP-MBD along the microtubule network were automatically detected. Then, the following parameters defining spatial segregation of two proteins were quantified: RFP/GFP fluorescence intensity in the spot, number of spots, width to length ratio of the spot, RFP/GFP fluorescence intensity in the cytoplasm. Fluorescence analysis included processing of signal by filtering out cells with low co-transfection level (RFP/GFP fluorescence intensity in the cytoplasm >5.8 in log scale) and spots with high width to length ratio (>0.22). The RFP/GFP fluorescence intensity of each spot was normalized to the value of RFP/GFP intensity in the cytoplasm. The data were presented in the scatterplots using MATLAB R2022a software (Figure S1C). The mixing scores (Figure 1C and S1C) were calculated as the squared value of the correlation coefficient (*corr* function in MATLAB R2022a software) showing how well the observed data fit the regression model (polynomial fitting shown on Figure S1C).

To measure the number of condensates per nucleus and FUS enrichment in nuclear condensates, nuclear condensates were automatically detected using the PerkinElmer Harmony v4.8 software. The following parameters were quantified: the number of nuclear condensates per well, the number of cells per well, FUS fluorescence intensity in the condensates, FUS fluorescence intensity in the nucleoplasm. The number of condensates per nucleus was calculated as the ratio of the number of nuclear condensates per well to the number of cells per well. The FUS enrichment in nuclear condensates was calculated as the ration of FUS fluorescence intensity in the condensates to FUS fluorescence intensity in the nucleoplasm. The data were presented in the univariate scatterplot by using *UnivarScatter* function in MATLAB R2022a software.

In silencing, overexpression and addback experiments the following parameters were quantified: nucleus size, distance between cells, HA-tagged protein nuclear fluorescence intensity, PAR nuclear fluorescence intensity. Relative increase in nuclear PAR level was calculated using MATLAB R2022a software as the increase in PAR nuclear fluorescence intensity signal for a window of HA-tagged protein expression (HA-tagged protein nuclear fluorescence intensity: 6.8–9 in log scale) compared to the PAR nuclear fluorescence intensity signal for the cells without HA-tagged protein overexpression (HA-tagged protein nuclear fluorescence intensity: <6.5 in log scale). The cells with abnormally small nuclei (<150 μm^2) and distance between the cells (<8 μm) were filtered out. The distribution of the relative increase in nuclear PAR level was presented as violin plots (Figures 2 and 5) by using *violinplot* function in MATLAB R2022a software.

Analysis of the level of protein PARylation *in vitro*

Bands of proteins labeled with [^{32}P]ADP-ribose were analyzed by using Quantity One Basic software (Bio-Rad). [^{32}P] NAD^+ signal intensity (arbitrary units, a.u.) of PARylated proteins was quantified as the raw signal of the smeared band corresponding to [^{32}P] PAR-labeled proteins minus the same-size background signal of gel in the respective lane. Data are presented as mean values ± SD. The quantitative data presented in histograms were obtained in at least three independent experiments.

Statistical analysis

All statistical tests were performed using MATLAB. The two-sample *t* test test was performed using the *ttest2* function. Significance levels were indicated as *p < 0.05, **p < 0.01, ***p < 0.001 and not significant (n.s.).